Facies (2023) 69:10
https://doi.org/10.1007/s10347-023-00667-6

ORIGINAL ARTICLE

Glendonite-bearing concretions from the upper Pliensbachian (Lower Jurassic) of South Germany: indicators for a massive cooling in the European epicontinental sea

Anna Merkel[1] · **Axel Munnecke**[1]

Received: 3 March 2023 / Accepted: 3 May 2023 / Published online: 18 May 2023

Abstract
The Pliensbachian–Toarcian transition was characterised by a drastic turnover from a cool climate to a period of rapid global warming. While the warming associated with the Early Toarcian Oceanic Anoxic Event is rather well-studied, the cause, intensity and extent of the preceding cooling in the late Pliensbachian are still discussed. Occurrences of glendonite play an important role in this debate, since glendonite is a pseudomorph after the cryophilic carbonate mineral ikaite. This study describes the first glendonite-bearing carbonate concretions from South Germany (Buttenheim clay pit, northern Franconian Alb), which represent the southernmost glendonite occurrence in the late Pliensbachian documented so far. Based on petrographical and sedimentological investigations as well as stable isotope analyses it is concluded that a low temperature was the main factor for ikaite formation in the studied section, suggesting that the late Pliensbachian cooling had a more far-reaching impact on the temperature of the European epicontinental sea than previously assumed. To explain the low temperatures required for ikaite precipitation, a model for the sea-ice driven formation of cold bottom-water masses on the continental shelf is proposed. The occurrence of several layers containing reworked hiatus concretions in the studied outcrop is interpreted as the result of recurrent sea-level falls caused by multiple glacial pulses characterising the overall cool climate in the late Pliensbachian.

Keywords Glendonite · Late Pliensbachian climate · Glaciation · Hiatus concretions · Stable isotopes

Introduction

The Jurassic has long been regarded as a period characterised by stable warm and humid greenhouse conditions with ice-free polar regions (e.g., Frakes et al. 1992). This picture has changed during the past decades (e.g., Dera et al. 2011). Especially the Early Jurassic was subject to pronounced climatic fluctuations with phases of rapid global warming, e.g., during the Sinemurian–Pliensbachian transition (Korte and Hesselbo 2011; Bodin et al. 2016; Schöllhorn et al. 2020a, b), at the Pliensbachian–Toarcian boundary (Korte and Hesselbo 2011; Bodin et al. 2016; Krencker et al. 2020), and in the early Toarcian during the Toarcian Oceanic Anoxic Event (T-OAE, also known as the Jenkyns Event; e.g., Jenkyns 1988, 2010; Suan et al. 2010; Dera et al. 2011; Müller et al. 2017). Between these warming events were intermittent phases of cooling, e.g., in the late Sinemurian (Peti and Thibault 2022) and in the late Pliensbachian (Price 1999; Donnadieu et al. 2011; Korte and Hesselbo 2011; Dera et al. 2011; Suan et al. 2011; Bougeault et al. 2017; Ruebsam et al. 2019; Ruebsam and Schwark 2021). Thus far, the focus of Early Jurassic climate research has been on the causes and consequences of hyperthermals, especially the T-OAE, leaving fundamental questions regarding the mechanisms controlling the cooling events and their impact on subsequent warmings unanswered (Korte et al. 2015; Schöllhorn et al. 2020a, b).

The assumption of a late Pliensbachian cooling is based on sedimentological and geochemical analyses as well as on palaeoecological investigations. Temperature reconstructions using $\delta^{18}O$ data of benthic and nektonic organisms suggest a water temperature between 10 and 15 °C in the European Realm (e.g., Dera et al. 2009; Korte et al. 2015; Gómez et al. 2016). However, absolute temperature

✉ Anna Merkel
anna.merkel@fau.de

[1] Friedrich-Alexander-Universität Erlangen-Nürnberg, GeoZentrum Nordbayern, Erlangen, Germany

reconstructions based on oxygen isotopes should be regarded with caution, since the $\delta^{18}O$ signature recorded in fossil hard parts not only depends on the temperature but also on evaporation rate and freshwater influx. Further indications for a rather dry and cool climate are offered by clay mineral ratio measurements (Bougeault et al. 2017; Schöllhorn et al. 2020a, b; Hollaar et al. 2022), as well as by $^{87}Sr/^{86}Sr$ ratios (Korte and Hesselbo 2011) and by variations in the phosphorus content (Schöllhorn et al. 2020b), which argue for a reduced continental runoff due to low weathering rates. Moreover, palaeontological and palaeoecological studies on marine organisms as well as on plant material reveal shifts in assemblages that point towards an adaptation of organisms to cooler temperatures (Zakharov et al. 2006; Arp and Seppelt 2012; Keupp and Schweigert 2017; Keupp 2021a).

The existence of polar ice caps during the late Pliensbachian is still debated. Sedimentological evidence arguing for the formation of ice sheets is provided by the occurrence of glacial deposits, such as dropstones, tillites and diamictites in high latitudes (Price 1999; Suan et al. 2011; Ruebsam and Schwark 2021), as well as by a prominent hiatus, which is interpreted as the result of a glacio-eustatic sea-level fall (Morard et al. 2003; Nordt et al. 2021). However, abundant fossil remains of marine reptiles in deposits from Siberia (Rogov et al. 2019; Zverkov et al. 2021) as well as palynological studies proving the presence of warm-adapted plant taxa in higher latitudes (Ilyina 1969; Rogov et al. 2019) contradict the idea of a permanent ice sheet.

Another important indicator for cold climate conditions is the presence of glendonites in several Pliensbachian sections, which occur as calcite pseudomorphs after the cryophilic mineral ikaite ($CaCO_3 \cdot 6H_2O$). Ikaite forms under natural conditions at temperatures of less than 9 °C (Marland 1975; Huggett et al. 2005; Selleck et al. 2007; Field et al. 2017). While the recent precipitation of ikaite in sea ice and cold seawater is well-studied (Dieckmann et al. 2008; Hu et al. 2014; Hu and Wang 2020), little is known about ikaite formation within sediments. The irregular temporal and spatial distribution of ikaite and glendonite suggests that a combination of different factors is required to trigger the precipitation of ikaite in addition to a low temperature (Rogov et al. 2021, 2023). It is assumed that a high alkalinity and an elevated phosphorus content are also important prerequisites (Kodina et al. 2003; Greinert and Derkachev 2004; Selleck et al. 2007; Zhou et al. 2015). The role of decomposing organic matter in the sediment column as a relevant factor is discussed as well (Muramiya et al. 2022).

The association of modern ikaite with low temperatures is the reason why the mineral and its pseudomorph are used as a proxy for cool water temperatures in the fossil record (e.g., Kaplan 1980; De Lurio and Frakes 1999; Swainson and Hammond 2001; Selleck et al. 2007; Rogov et al. 2017, 2023; Vickers et al. 2022). Late Pliensbachian glendonites are documented in Siberia, Russia, representing polar palaeoenvironments (e.g., Kaplan 1978; Suan et al. 2011; Nikitenko et al. 2013; Rogov 2015; Morales et al. 2017) but also in mid-latitude sections in northern Germany (Teichert and Luppold 2013; Zimmermann et al. 2015; Barth et al. 2018; van de Schootbrugge et al. 2019). Since glendonite is a pseudomorph, it shows a distinct internal fabric which is produced when the water-rich ikaite dehydrates and transforms into calcite leading to a loss of up to one-third of the initial crystal volume (Selleck et al. 2007). The resulting fabric consists of granular calcite overgrown by various cement generations (Boggs 1972; Kaplan 1980; Larsen 1994; McLachlan et al. 2001; Greinert and Derkachev 2004; Huggett et al. 2005; Selleck et al. 2007; Teichert and Luppold 2013; Scheller et al. 2022) which is termed "guttulatic microfabric", adapted after "guttula", the Latin word for "very small droplet" (Scheller et al. 2022).

However, the use of glendonite as a temperature proxy has been challenged by several authors showing that the precipitation of ikaite can be triggered under laboratory conditions at temperatures above its assumed stability window (Clarkson et al. 1992; Rodríguez-Ruiz et al. 2014; Purgstaller et al. 2017; Stockmann et al. 2018; Tollefsen et al. 2020). This raises the question as to whether the occurrence of glendonite in mid-palaeolatitude sections de facto documents a drastic temperature decrease in temperate areas. Instead, methane seepage has been proposed as a trigger for precursor ikaite growth in several late Pliensbachian successions (Teichert and Luppold 2013; Morales et al. 2017; van de Schootbrugge et al. 2019), since a favouring influence of methane has been observed in modern ikaite formation (Schubert et al. 1997; Kodina et al. 2003; Krylov et al. 2015).

This study describes the first Pliensbachian glendonites from South Germany which were found in carbonate concretions from the Buttenheim clay pit, Bavaria, representing the most southern glendonite occurrence in this time slice so far recorded. The glendonite-bearing interval occurs right below the Pliensbachian–Toarcian boundary which is characterised by a pronounced hiatus. The presence of reworked carbonate concretions in several layers below the glendonite-bearing interval documents recurrent sea-level falls throughout the studied succession. Combining investigations on the sedimentological features present in the reworked intervals with a petrographic analysis of the glendonite-bearing concretions and stable isotope data, this study aims to answer the question as to how significant the temperature decrease in the European epicontinental sea was during the late Pliensbachian cooling.

Geological setting

The studied material was sampled in the Buttenheim clay pit located at the western margin of the northern Franconian Alb in Bavaria, South Germany (Fig. 1a; 49° 47′ 40.7″ N/11° 02′ 44.0″ E). The Franconian Alb is a low mountain range consisting of gentle southward dipping sedimentary rocks of Early to Late Jurassic age (Fig. 1a). The deposition of Jurassic strata started with the flooding of the shelf area between Eurasia and Laurentia from a north-eastern direction at the Triassic–Jurassic transition (Richter 1985). On the drowned shelf, now forming the European epicontinental sea, land masses of various dimensions persisted (Fig. 1b, c). Towards the south, the shelf transitioned into the Tethys Ocean, whereas the Viking Corridor connected the European Realm with the Arctic Realm (Fig. 1b, c) (Surlyk 2003; Korte et al. 2015).

The study area was located close to the Bohemian Massif and the Vindelician Land in the eastern part of the epeiric sea (Fig. 1c) (Richter 1985; Meyer and Schmidt-Kaler 1992). During the late Early Jurassic, the basin deepened and the terrestrial influence decreased which resulted in the deposition of thick, monotonous successions consisting of claystones and marlstones (Meyer and Schmidt-Kaler 1992).

The section exposed in the Buttenheim clay pit encompasses the upper part of the Pliensbachian Amaltheenton Formation, including the uppermost *Amaltheus margaritatus* Zone and large parts of the *Pleuroceras spinatum* Zone. The approx. 36 m thick Pliensbachian succession is overlain by the lower part of the Toarcian Posidonienschiefer Formation with a thickness of about 4 m (Fig. 2a, b).

Pliensbachian strata consist of dark, fossiliferous clays with abundant limestone concretions of various shapes and sizes. A special feature of the Buttenheim clay pit is the preservation of aragonite which can be observed in many mollusc shells. Previous studies of the fossil assemblage revealed a high biodiversity in both nektonic and benthic communities indicating a well-oxygenated water column and an adequate nutrient supply. Different species of ammonites, belemnites and fish (Keupp and Schweigert 2017; Keupp and Fuchs 2020; Keupp 2021b) as well as larger predators such as ichthyosaurs and sharks populated the water column, whereas the seabed was the habitat of numerous epifaunal organisms adapted to a rather soft seafloor, such as gastropods, bivalves, foraminifera, sea urchins, holothurians, ophiuroids, ostracods and decapod crustaceans (Nützel and Gründel 2015; Keupp and Doppelstein 2018; Karapunar et al. 2020; Kutscher and Reich 2021; Keupp and Schweigert 2021). The fine-grained sediment itself provided a protected habitat for numerous species of infaunal molluscs and annelid and polychaete worms (Nützel 2007). The colonisation of the seafloor resulted in strong bioturbation which is well visible in early diagenetic concretions (Munnecke and Merkel 2021). Excremental remains (faecal pellets) produced by sediment-feeding organisms can be found in high abundance inside ammonite shells (Munnecke and Merkel 2021). Since the depositional area was located close to the Bohemian Massif in the west, pieces of driftwood of varying sizes can be observed in the outcrop which served as floating substrates for sessile organisms (Keupp et al. 2018).

Furthermore, the succession is characterised by multiple intervals featuring so-called "hiatus concretions" sensu Voigt 1968; (Keupp and Schobert 2015; Keupp 2021c; Munnecke and Merkel 2021) which formed when the overlying sediment was removed due to elevated water energy. The exhumed concretions were later colonised and bioeroded by different organisms including crinoids, brachiopods, serpulids, gastropods, bivalves, sea urchins and polychaete worms (Keupp 2021c). Four intervals with hiatus concretions are identified in the Buttenheim clay pit so far (Fig. 2a, b). The first interval is called the "Pyriterzbank" and is located at the *A. margaritatus*/*P. spinatum* Zone boundary. The second interval is the "Quellhorizont" followed by the "Echiniden-Pectiniden-Horizont" and the "Bollernbank" limestone bed at the Pliensbachian–Toarcian transition (Fig. 2c, d).

The overlying Toarcian succession is dominated by finely laminated bituminous marls ("paper shales") which contain large micritic concretions (Fig. 2b, c). Marls and concretions lack a benthic fauna but contain planktic gastropods and fish remains. This indicates hostile conditions prevailing at the seafloor. The succession terminates at the top of a sedimentary package consisting of four limestone beds each of 20 to 30 cm thickness, which include the so-called "Inoceramenbank" bed at the bottom and the "Monotis-Dactyliocerasbank" bed at the top (Fig. 2b).

Materials and methods

About 200 discus-shaped concretions were collected in the uppermost part of the Pliensbachian succession in the Buttenheim clay pit. Approximately half of the collected concretions were cut to check for the presence of glendonite. The largest crystal aggregates were chosen for different petrographic and geochemical analyses. In addition, material from the overlying "Bollernbank" bed, as well as hiatus concretions from slightly older strata ("Pyriterzbank", "Quellhorizont" and "Echiniden-Pectiniden-Horizont") were studied for their sedimentological features.

Microfacies analysis was carried out on 21 thin sections produced from 21 different glendonite-bearing concretions

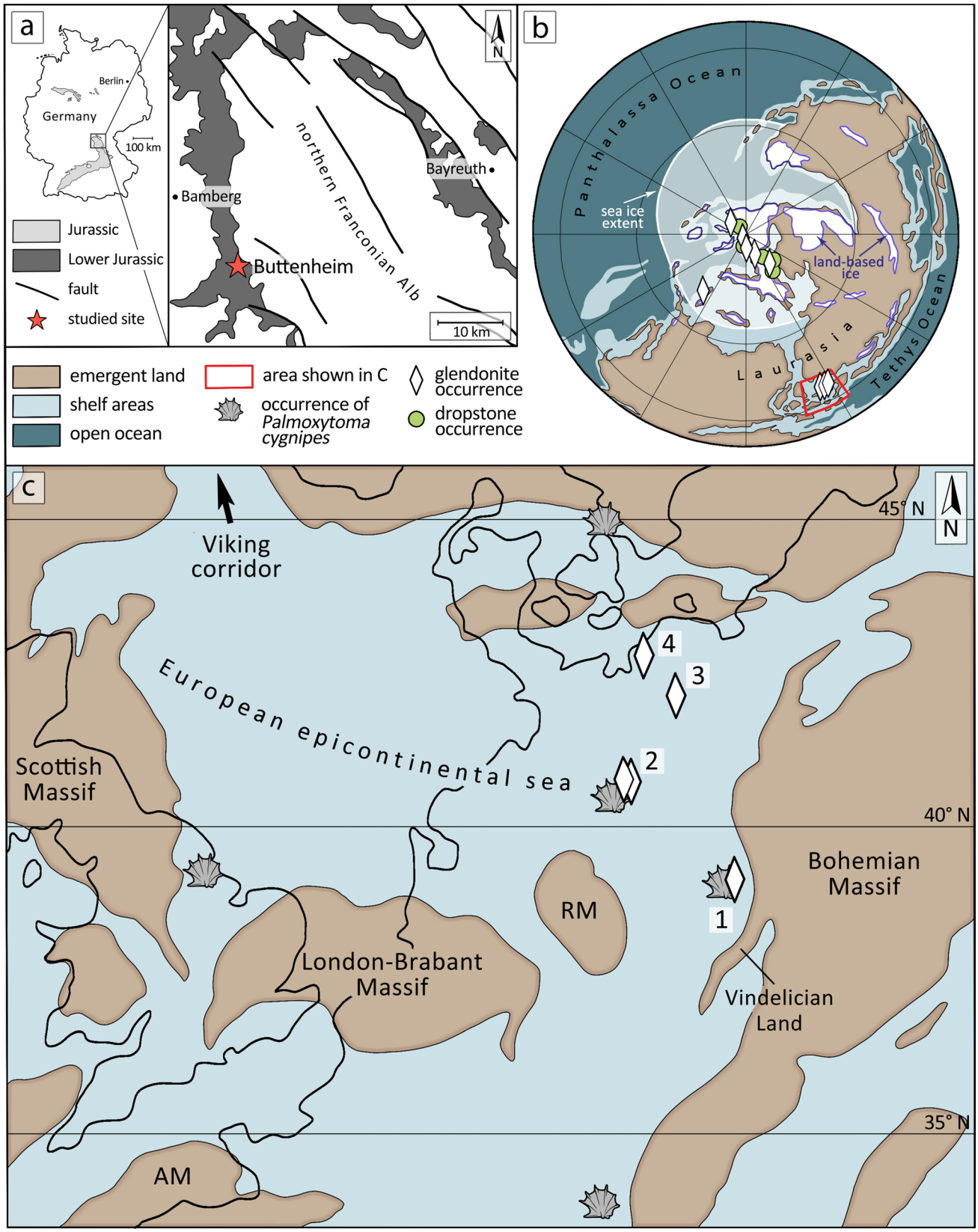
a
Berlin
Germany
100 km
Jurassic
Lower Jurassic
fault
studied site
N
Bamberg
Buttenheim
Bayreuth
northern Franconian Alb
10 km
b
Panthalassa Ocean
sea ice extent
land-based ice
Laurasia
Tethys Ocean
emergent land
shelf areas
open ocean
area shown in C
occurrence of Palmoxytoma cygnipes
glendonite occurrence
dropstone occurrence
c
Viking corridor
45° N
N
European epicontinental sea
4
3
2
1
Scottish Massif
40° N
Bohemian Massif
RM
London-Brabant Massif
Vindelician Land
35° N
AM

◂**Fig. 1** Location, geological and palaeogeographic setting of the study area. **a** Left: outline of Germany with outcropping Jurassic strata; right: geological map of the Northern Franconian Alb (redrawn after Meyer and Schmidt-Kaler 1992) with the location of the Buttenheim clay pit (red star). **b** Palaeogeographic map of the northern hemisphere in the late Pliensbachian including occurrences of dropstones and glendonites (redrawn after Ruebsam et al. 2019 and Ruebsam and Schwark 2021) and a reconstruction of the possible sea-ice extent as well as areas covered by land-based ice (redrawn after Ruebsam and Schwark 2021). **c** Palaeogeography of the European epicontinental sea in the late Pliensbachian (redrawn after Blakey 2016) with occurrences of glendonite (1: new occurrence in Buttenheim (this study); 2: Cremlingen/Schandelah near Braunschweig (Teichert and Luppold 2013; van de Schootbrugge et al. 2019); 3: Goldberg near Schwerin (Zimmermann et al. 2015); 4: Barth near Stralsund (Barth et al. 2018)) and sites with specimens of *Palmoxytoma cygnipes* (Arp and Seppelt 2012; Schweigert 2019). *AM* Amorican Massif, *RM* Rhenish Massif

(Table 1). Serial thin section of samples from the "Quellhorizont", the "Echiniden-Pectiniden-Horizont", and the "Bollernbank" reworked intervals were available in the teaching collection of the GeoZentrum Nordbayern (Friedrich-Alexander-Universität Erlangen-Nürnberg) (Table 1). The photomicrographs were generated with a Zeiss Axio. Zoom.V16 binocular and a Zeiss Axio Imager.M2m microscope. The devices are equipped with Zeiss camera models Axiocam 506 color and Axiocam 305 color.

In addition to the transmitted light microscopy investigation, an element composition analysis was carried out on two glendonite samples using a TESCAN Vega.xmu scanning electron microscope coupled with an energy dispersive X-ray spectroscopy device operated with an acceleration voltage of 20 kV.

For $\delta^{13}C$ and $\delta^{18}O$ analyses, 18 samples were manually drilled from cut glendonite aggregates (Table 1). The samples were reacted with 100% phosphoric acid at 70 °C using a Gasbench II connected to a ThermoFisher Delta V Plus mass spectrometer. All values are reported in per mil relative to Vienna Pee–Dee Belemnite (VPDB). Reproducibility and accuracy were monitored by replicate analysis of laboratory standards calibrated by assigning a $\delta^{13}C$ of + 1.95‰ VPDB to NBS19 and − 47.3‰ VPDB to IAEA-CO9 and a $\delta^{18}O$ of − 2.20‰ VPDB to NBS19 and − 23.2‰ VPDB to NBS18. Reproducibility for $\delta^{13}C$ and $\delta^{18}O$ was ± 0.07‰ VPDB and ± 0.02‰ VPDB, respectively.

Results

Field observations

The Pliensbachian succession exposed in the Buttenheim clay pit consists of monotonous clays with abundant carbonate concretions of which some show signs of reworking ("hiatus concretions"; Voigt 1968). So far, four hiatus concretion-bearing layers are described in Buttenheim (Fig. 2a, b). Three layers date to the late Pliensbachian ("Pyriterzbank", "Quellhorizont" and "Echiniden-Pectiniden-Horizont"), whereas the fourth reworked interval marks the Pliensbachian–Toarcian transition ("Bollernbank" limestone bed).

The Pliensbachian reworked intervals share several features. First, the hiatus concretions are surrounded by fossiliferous clays (Fig. 3a). In view of the large amount of fine-grained shell material, these layers appear lighter in colour compared to the non-reworked clays above and below. In addition, all hiatus concretions show bioeroded surfaces with numerous holes and indentations produced by boring and grazing organisms (Fig. 3a, b). An overgrowth by calcareous tube worms is particularly common for concretions from the "Echiniden-Pectiniden-Horizont" interval (Fig. 3b). The interior appears structureless and is often devoid of macrofossils. Significant differences between the reworked intervals can be noted in size and shape of the hiatus concretions. Specimens from the "Pyriterzbank" interval are rather small (only a few millimetres to centimetres in diameter, rarely up to a decimetre), show a dark grey colour and commonly have a spherical shape. The surrounding bioclast-rich layer has a thickness of a few centimetres. The concretions of the "Quellhorizont" interval have a similar size and shape to those from the "Pyriterzbank", but appear brownish (Fig. 3a). The "Echiniden-Pectiniden-Horizont" interval is characterised by rather large concretions (few centimetres to several decimetres in size) which commonly have an elongate, irregular shape with a light grey coloured surface (Fig. 3b).

The youngest reworked interval in the Buttenheim clay pit marks the transition from the Pliensbachian to the Toarcian and is called the "Bollernbank" bed (Fig. 2c, d). The spherical-shaped hiatus concretions from this interval are dark grey in colour, but if the surface is weathered they appear brownish (Fig. 4a, b). These concretions are almost devoid of macrofossils, but have a strongly bioeroded exterior (Fig. 4b). They are imbedded in a light brownish limestone matrix with abundant belemnite rostrums (Fig. 4b) which commonly show signs of reworking. Crustacean burrows are another typical feature (Fig. 4a).

In a layer located ca. 30–40 cm below the "Bollernbank" limestone bed glendonite-bearing concretions occur (Fig. 2b, c, e). This specific concretion type is restricted to a single layer and differs from the other carbonate concretions present in the Buttenheim clay pit. The glendonite-bearing concretions have a very similar, flat, discus-like shape with a regular and smooth surface (Figs. 2e, 5a–e). In view of their special and unique shape, they are informally referred to as "discus concretions". Another feature is the constant size with about 6 cm diameter on average. The smooth surface is light grey in colour, whereas the interior is rather

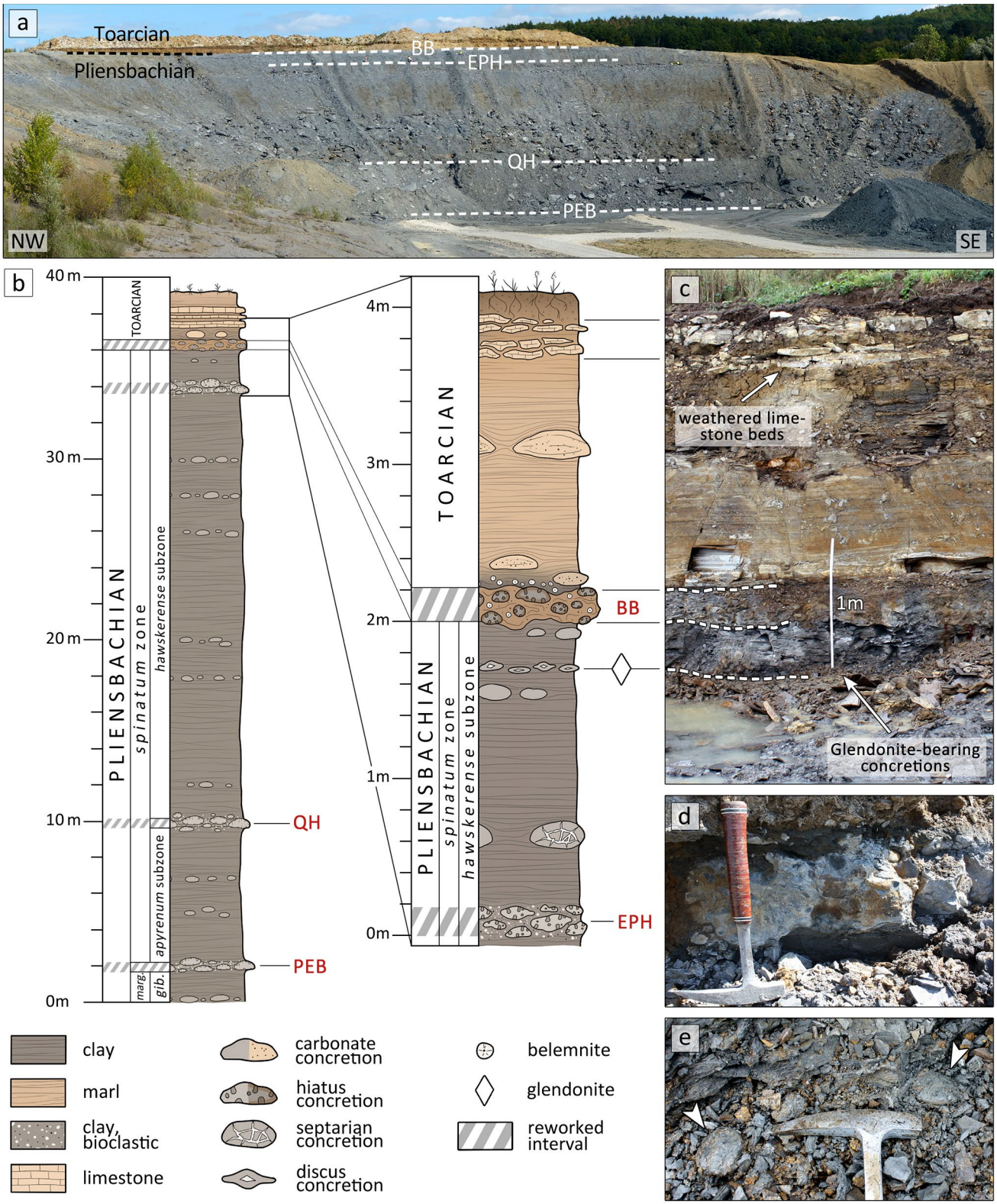

brownish. In most cases, a pyritized cortex with a thickness of about 1–2 cm is present (Fig. 5d, f). In some cases, pyrite nodules can be observed on the surface (Fig. 5e). The glendonite-bearing concretions show no signs of reworking and are devoid of macrofossils except for rare ammonite shells (Fig. 5c).

Almost every discus-shaped concretion from the relevant interval contained a glendonite aggregate. They mostly

◂**Fig. 2** Stratigraphy of the Buttenheim clay pit. **a** Panorama showing the north-eastern slope of the clay pit with the position of the Pliensbachian–Toarcian boundary and the so far known reworked intervals marked by the presence of hiatus concretions (PEB = "Pyriterzbank"; QH = "Quellhorizont"; EPH = "Echininden-Pectiniden-Horizont"; BB = "Bollernbank" limestone bed). **b** Left: stratigraphic column of the Lower Jurassic exposed in Buttenheim (redrawn after Keupp and Schobert 2015); right: detailed column of the uppermost part of the section (abbreviations: gib. = *Amaltheus gibbosus* Subzone; marg. = *Amaltheus margaritatus* Zone). **c** Field photograph of the uppermost part of the section exposing the Pliensbachian–Toarcian boundary. **d** Field photograph of the "Bollernbank" bed marking the Pliensbachian–Toarcian transition. **e** Field photograph of two discus-shaped concretions recovered ca. 30 cm below the "Bollernbank" bed

occur in the centre of the concretions and are not visible from the outside. They are a few millimetres in size (up to 20 mm, ca. 6 mm on average), appear bright, and commonly show a rhombic outline as well as a yellowish carbonate crust between the glendonite aggregate and the surrounding concretion (Fig. 5f).

Microfacies analysis

Reworked intervals

Hiatus concretions from the Pliensbachian reworked intervals consist of homogeneous micrite (Fig. 3c). Structures such as stratification were not observed, but in some cases burrows are visible. Smaller fossils or fragments of shells are locally incorporated in the micritic material. Bioerosion traces of various shapes and sizes characterise the surfaces of the concretions (Fig. 3c). In thin sections produced from material sampled in the "Quellhorizont" interval, microbial structures overgrowing hiatus concretions and ammonite shell fragments are an often-observed feature (Fig. 3d). The matrix in which the concretions are embedded consists of densely packed shell fragments (Fig. 3c) derived by various organisms, such as ammonites, gastropods, bivalves, echinoderms and brachiopods. Ostracods and foraminifera also occur. The space between the poorly sorted bioclasts is filled with micrite (Fig. 3c). Detrital quartz grains can be found in the surrounding sediment as well. In samples obtained from the "Quellhorizont" interval, distinct layers consisting of silt-sized quartz grains were observed (Fig. 3e). Pyritisation of hiatus concretions, matrix and shell fragments can occur (Fig. 3c).

The hiatus concretions of the "Bollernbank" limestone bed resemble other concretions from the Pliensbachian of Buttenheim with respect to matrix and fossil content. They consist of homogeneous, almost structureless micrite and show strongly bioeroded surfaces (Fig. 4c). In contrast to the almost fossil-free hiatus concretions, the surrounding limestone matrix is very rich in biogenic components, such as fragments of echinoderms, mollusc shells, brachiopods and foraminifera (Fig. 4c, e–g). Belemnite rostrums are particularly common and commonly show various bioerosion traces penetrating the guards (Fig. 4d). The bioclasts are relatively well-sorted (Fig. 4e, f). Abundant bioturbation traces (Fig. 4e) and a random distribution of components (Fig. 4f) suggest a high degree of sediment mixing. In some areas, the micrite content decreases significantly and the formation of a fitted fabric can be observed which is characterised by stylolitic contacts between the calcitic components (Fig. 4g). Similar to the Pliensbachian reworked intervals, microbial structures (Fig. 4h) and pyritisation of components and matrix (Fig. 4c, d, f) are common in this interval.

Glendonite-bearing concretions

Except for the glendonite aggregates the interior of the glendonite-bearing concretions only shows few features. Rarely, gastropods, benthic foraminifera, echinoderm fragments and pyritized sponge needles are present in the micritic matrix of the concretions. Peloids were observed, as well as remains of degraded organic matter and small fragments of plant material. The matrix consists of homogeneous micrite which appears brownish to yellowish (Fig. 6a, c–e). Pyrite occurs either finely distributed or as framboids. The pyrite content increases towards the concretion margin, forming a cortex which appears opaque in transmitted light (Fig. 6a) and yellowish to golden in reflected light (Fig. 6b). Sedimentary structures such as stratification or bioturbation traces are not evident, suggesting a high degree of mixing by endobenthic organisms.

The microscopic examination of the glendonites shows that the crystal aggregates can have various outer shapes (Fig. 6c–e). A rhombic outline, which is characteristic for glendonite, is present in many cases (Fig. 6c, d) as well as rather roundish forms or irregular structures (Fig. 6e). Almost half of the investigated glendonite aggregates have a carbonate crust which usually traces the outline of the former ikaite crystal (external crust, Fig. 6d). However, it can also occur within the glendonite aggregates (internal crust, Fig. 6c). The crust commonly shows a distinct layering, which in some cases has a cauliflower-like growth, resembling a microbial carbonate crust (Fig. 6f). The contact between the glendonite aggregates and the surrounding micrite of the concretions is either smooth (especially, if an external crust is present, Fig. 6c, d) or irregular with individual calcite crystals extending into the micritic matrix (Fig. 6e).

The internal structure of the glendonite aggregates is characterised by a guttulatic microtexture which consists of hexagonal to spherical shaped crystal cores and an overgrowth with one or multiple cement generations. This diagnostic fabric is developed in varying degrees in all studied samples.

Table 1 List of samples chosen for microfacies analysis, SEM and EDX analysis and stable carbon and oxygen isotopy

Purpose	Number of samples	Sample tags	Interval	Age	Studied material
Thin section analysis	1 sample, 14 sections	AM 533	QH	Pl; lower *P. spinatum* Zone	Hiatus concretions; surrounding sediment
	1 sample, 20 sections	AM 531	EPH	Pl; upper *P. s pinatum* Zone	Hiatus concretions, surrounding sediment
	21 samples, 21 sections	BU-G-1 to BU-G-20; M-BU-77b	GL	Pl; uppermost *P. spinatum* Zone	Glendonites; surrounding concretions
	3 samples; 24 sections	AM 547; M-BU-13; M-BU-79	BB	Pl-To boundary	Hiatus concretions; surrounding limestone matrix
EDX analysis	2 samples	BU-G-2; BU-G-19	GL	Pl; uppermost *P. spinatum* Zone	Glendonites
Stable isotope analysis	18 samples; 18 analyses	Iso-G-1 to Iso-G-18	GL	Pl; uppermost *P. spinatum* Zone	Glendonite

BB "Bollernbank" limestone bed, *EPH* "Echiniden-Pectiniden-Horizont", *GL* glendonite-bearing interval, *Pl* Pliensbachian, *QH* "Quellhorizont", *To* Toarcian; samples tagged with "AM" were part of the teaching collection of the GeoZentrum Nordbayern, Friedrich-Alexander-Universität Erlangen-Nürnberg

The first calcite generation forms granular crystals of various shapes, for example, elongate (Fig. 7a, c), spherical to subspherical (Fig. 7a, c, e, f), hexagonal (Fig. 7e) or irregular (Fig. 7a, c, e–g). Twinning is also a frequently observed phenomenon (Fig. 7c, h). In some cases, crystals can have a shape similar to the stellate growth form of the former ikaite (Fig. 7f). The second cement generation forms an isopachous rim around the first calcite phase (Fig. 7a, c, e). In crossed-polarised light, most cement rims show a syntaxial extinction behaviour (Fig. 7b, d). However, the second cement generation can be replaced by a thin, brownish rim (Fig. 7f–h). Multiple cement overgrowths result in the formation of a zonation (Fig. 7a, g). The remaining pore space can be filled by various materials, for example, by clear calcite spar (Fig. 7a, c, e, f, h), by pyrite (Fig. 7f), or by both (Fig. 7h). Filling of pore space by micrite was also observed (Fig. 7a, f).

EDX analyses

EDX analysis of two glendonite aggregates reveals that the crystal cores as well as the surrounding cement generations consist of low magnesium calcite (LMC). Spot analyses of the crystal margins show a slight increase of iron, manganese and magnesium.

Stable isotope analysis

Carbon isotope values obtained from glendonite aggregates range from − 21.8 to − 10.3‰ VPDB (mean: − 15.6‰ VPDB) (Table 2, Fig. 8). For $\delta^{18}O$, the values vary between − 9.4 and − 3.6‰ VPDB (mean: − 5.8‰ VPDB).

Discussion

Reconstruction of the depositional environment

Studies dealing with the Buttenheim succession so far have focused on the abundant and excellently preserved fossils (e.g., Nützel and Gründel 2015; Keupp and Schweigert 2017; Keupp and Doppelstein 2018; Karapunar et al. 2020; Keupp and Fuchs 2020; Kutscher and Reich 2021; Keupp and Schweigert 2021). The diverse nektonic, endo- and epibenthic fauna suggests that the water column as well as the uppermost part of the sediment were well-oxygenated. However, further information about the depositional environment is difficult to obtain, since successions consisting of monotonous clays commonly lack macroscopic sedimentary structures. In view of the fine-grained, homogeneous nature of the clay the preservation of such features is limited, making it almost impossible to gain information about water energy, sea-level fluctuations and climatic conditions in the field. In addition, bioturbation and later compaction could easily have destroyed any primary structures. This makes further investigations necessary. For example, syn-sedimentary features can be preserved inside carbonate concretions which form during early diagenesis in the shallow subsurface. Fortunately, the Buttenheim clay pit has large numbers of such early diagenetic concretions to offer for microscopic investigations.

Structures such as cross-stratification, orientation of components or fining-upward tendencies were not observed in the studied concretions. This either means that these structures never formed or that strong bioturbation homogenised the sediment. The poor sorting of biogenic components and the lack of rounded bioclasts supports the first assumption, indicating that the seafloor was located below storm wave

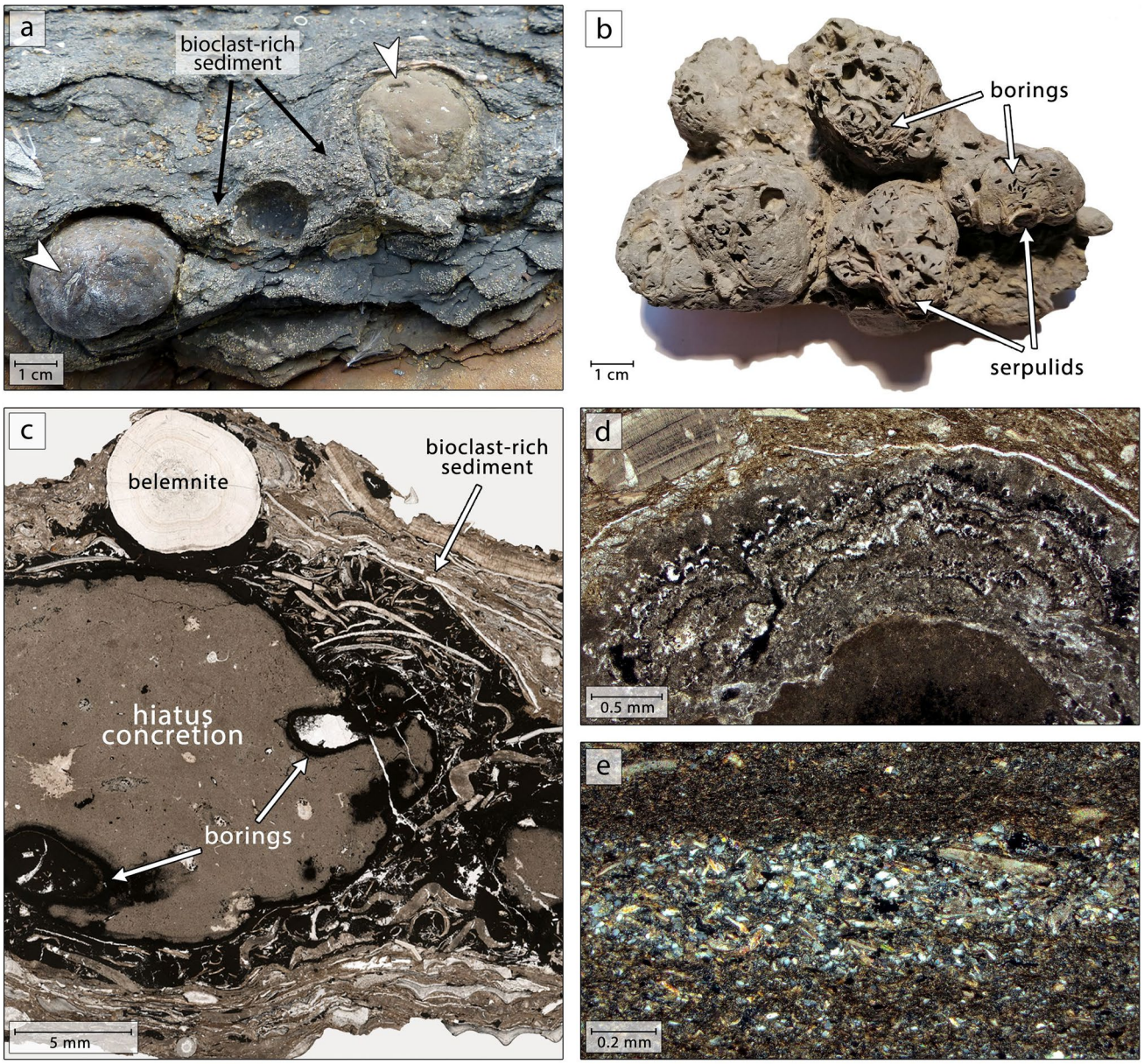

Fig. 3 Characteristics of the upper Pliensbachian reworked intervals exposed in the Buttenheim clay pit. **a** Field photograph of two hiatus concretions embedded in a bioclast-rich clay matrix; white arrows highlight borings on the concretion surfaces; "Quellhorizont" reworked interval, lower *P. spinatum* Zone. **b** Hiatus concretion with bioerosion traces and extensive serpulid overgrowth; "Echiniden-Pectiniden-Horizont" reworked interval, uppermost *P. spinatum* Zone. **c** Photomicrograph of a bored and partly pyritised hiatus concretion embedded in a poorly sorted matrix consisting of shell fragments and micrite; "Echiniden-Pectiniden-Horizont" reworked interval, uppermost *P. spinatum* Zone, thin section no. AM 531. **d** Photomicrograph of a microbial overgrowth on a hiatus concretion; "Quellhorizont" reworked interval, lower *P. spinatum* Zone, thin section no. AM 533. **e** Photomicrograph of a quartz-rich layer within the bioclastic sediment; "Quellhorizont" reworked interval, lower *P. spinatum* Zone, thin section no. AM 533, crossed-polarised light

base for most of the time. However, the calm conditions were interrupted by recurrent phases characterised by elevated water energy. This change is documented by the occurrence of hiatus concretions in certain layers (Figs. 2b, 3a, b, 4a, b). This type of concretion forms due to winnowing of the overlying sediment and a subsequent sedimentation gap (Voigt 1968; Sadlok and Zatoń 2020). Hiatus concretions offer important hardgrounds for sessile organisms, for example, serpulids (Fig. 3b) and microbes (Figs. 3d, 4h). Polychaete worms produced large, pear-shaped borings (Figs. 3b, c, 4b, c). Bioerosion of ammonite shells and belemnite rostrums can be observed as well, especially in the "Bollernbank" limestone bed (Fig. 4d). Shell concentrations surrounding the hiatus concretions suggest a significant increase in water

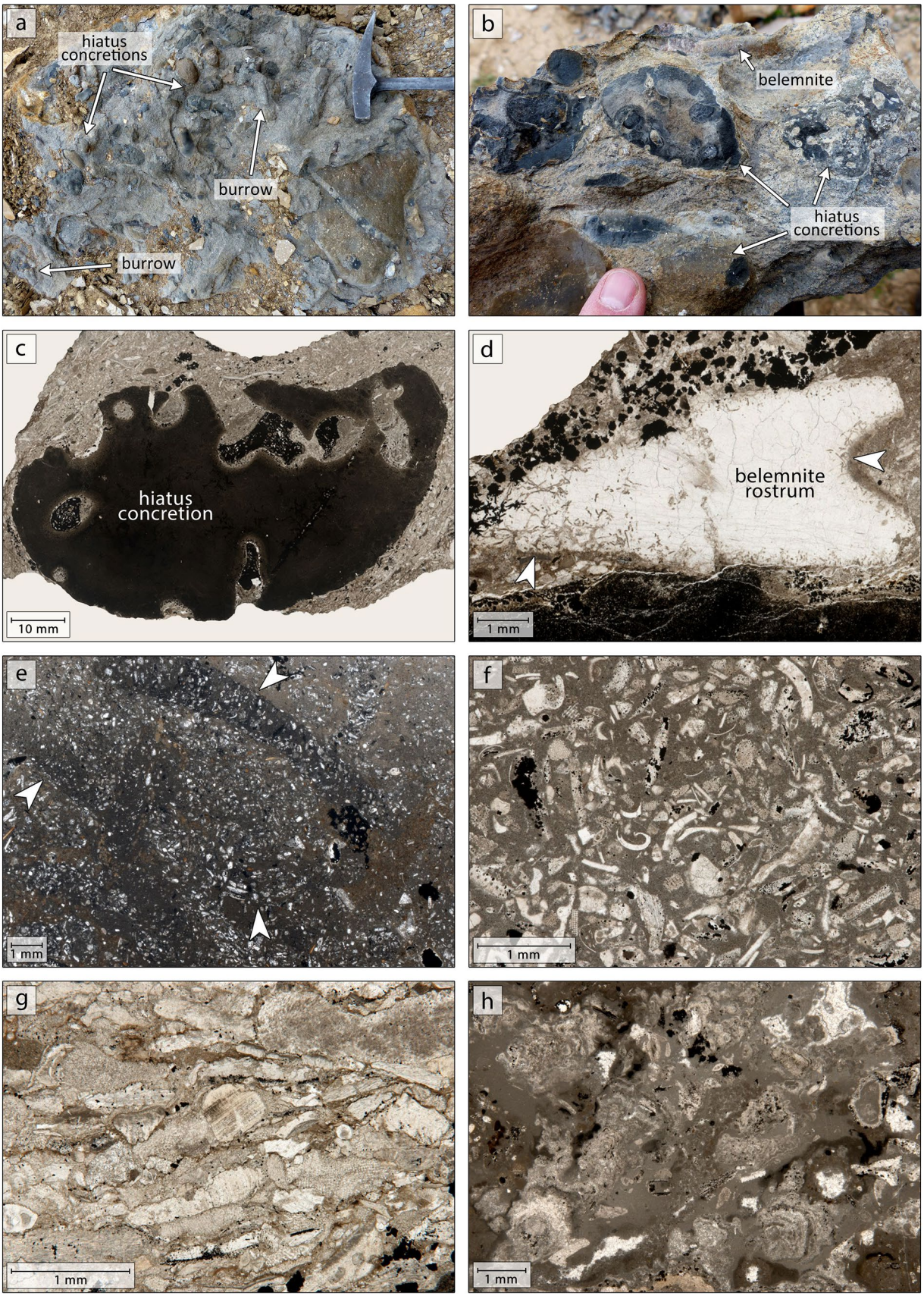
a
hiatus concretions
burrow
burrow
b
belemnite
hiatus concretions
c
hiatus concretion
10 mm
d
belemnite rostrum
1 mm
e
1 mm
f
1 mm
g
1 mm
h
1 mm

◂**Fig. 4** Characteristics of the "Bollernbank" limestone bed (Pliensbachian–Toarcian transition). **a** Bedding plane with abundant hiatus concretions and crustacean burrows. **b** Hand specimen with strongly bioeroded concretions in a micritic matrix. **c** Photomicrograph of a bored hiatus concretion embedded in a fine-grained bioclastic matrix; thin section no. AM 547. **d** Photomicrograph of a bioeroded belemnite rostrum; arrows indicate thin borings; thin section no. AM 547. **e** Photomicrograph of the bioturbated bioclast-rich matrix surrounding the hiatus concretions; arrows indicate bioturbation traces; thin section no. M-BU-13. **f** Photomicrograph of the matrix surrounding the hiatus concretions; note the good sorting of components (mainly fragments of echinoderms, foraminifera, mollusc shells and brachiopods); thin section no. AM 547. **g** Photomicrograph of echinoderm fragments and foraminifera forming a fitted fabric; note the stylolitic contacts between the components and the absence of micrite; thin section no. AM 547. **h** Photomicrograph of microbial structures in the micritic matrix surrounding the hiatus concretions; thin section no. M-BU-79

energy (Figs. 3a, c, 4c, e, f). In some bioclastic parts of the "Bollernbank" bed, the energy was sufficient enough to wash out the micritic matrix. The lack of fine-grained material in between the bioclasts led to the formation of a fitted fabric caused by compaction prior to lithification (Fig. 4g).

Possible causes for the recurrent changes in water energy as well as the implications resulting from the discovery of glendonite in Buttenheim on the late Pliensbachian climate are discussed in the following sections.

The ikaite–glendonite transformation

All studied glendonites show a guttulatic microfabric. This characteristic paragenetic sequence is produced when the precursor ikaite is removed from its stability window and starts to disintegrate. Several authors have noted that up to three calcite generations were formed during the ikaite–calcite transformation (Boggs 1972; Kaplan 1980; Larsen 1994; McLachlan et al. 2001; Greinert and Derkachev 2004; Huggett et al. 2005; Selleck et al. 2007; Teichert and Luppold 2013; Scheller et al. 2022). The first phase forms during the dehydration of ikaite and is termed "replacive calcite" or "primary calcite" which consists of granular crystals. The second phase is an isopachous, in some cases syntaxial, cement rim which encloses the replacive calcite. The third and final cement generation fills the remaining pore space. All three calcite generations were observed in the Buttenheim glendonites. The replacive calcite is formed by calcite crystals of various shapes (Fig. 7a, c, e) which are overgrown by a (syntaxial) cement generation (Fig. 7a–d). Remaining pore space is filled by clear calcite spar (Fig. 7a, c, e) and/or by pyrite (Fig. 7f, h).

Element distribution analysis shows that the first calcite generation in the Buttenheim glendonites is composed of LMC which is in line with previous studies on the elemental composition of glendonites (e.g., Greinert and Derkachev 2004; Huggett et al. 2005; Selleck et al. 2007; Teichert and Luppold 2013). The low concentration of other elements in the first calcite generation is probably due to the fact that the precursor ikaite did not incorporate high amounts of magnesium or iron (Schubert et al. 1997). Since the first calcite phase is assumed to precipitate directly from carbonate released during the disintegration of the former ikaite, the element concentrations of the resulting calcite were probably similar (Selleck et al. 2007; Teichert and Luppold 2013). In the Buttenheim samples, only a slight increase of iron, magnesium and manganese was observed towards the margins of the first calcite generation and the overgrowth. This contrasts with findings of other authors who noted that the second and the third cement generation show significantly elevated contents of iron, magnesium and manganese or even consist of HMC or siderite (e.g., Greinert and Derkachev 2004; Huggett et al. 2005; Selleck et al. 2007; Teichert and Luppold 2013). This suggests that the changes in the chemical composition of the pore water during the precipitation of the different cement generations were only of minor significance which argues either for very stable conditions in the subsurface or for a rapid growth of the entire paragenetic sequence.

The presence of carbonate crusts inside and outside the studied glendonite specimens is a rarely observed phenomenon in ancient glendonites. Such macro-zoned glendonites are so far only known from the Hauterivian of Svalbard (Vickers et al. 2018) and from Middle Jurassic deposits from the Barents Sea shelf (Mikhailova et al. 2021). Proposed formation mechanisms are oscillating changes of the chemical and thermal conditions in the shallow subsurface (Vickers et al. 2018) as well as the activity of microbial overgrowths combined with the mixture of seawater and pore water (Mikhailova et al. 2021). Whether one of the proposed models applies to the glendonites presented in this study or whether a previously unknown mechanism was involved in the formation of the macro-zoned glendonite aggregates, must be revealed by future research, since detailed analyses of the formation mechanisms of the Buttenheim glendonites are beyond the scope of this study.

Was methane involved in the formation of the Buttenheim ikaites/glendonites?

Studies on recent ikaites suggest that elevated alkalinities, which favour the precipitation of carbonate minerals, and an elevated phosphorus content, which inhibits the growth of calcite, are important factors for ikaite formation in addition to low temperatures (Kodina et al. 2003; Greinert and Derkachev 2004; Selleck et al. 2007; Zhou et al. 2015). Such conditions prevail in the sulphate reduction zone and in the zone of anaerobic oxidation of methane (AOM) in fine-grained, organic-rich sediments. Therefore, it is assumed that these zones are most likely the intervals in which the formation of ikaite takes place (Kodina et al. 2003; Greinert

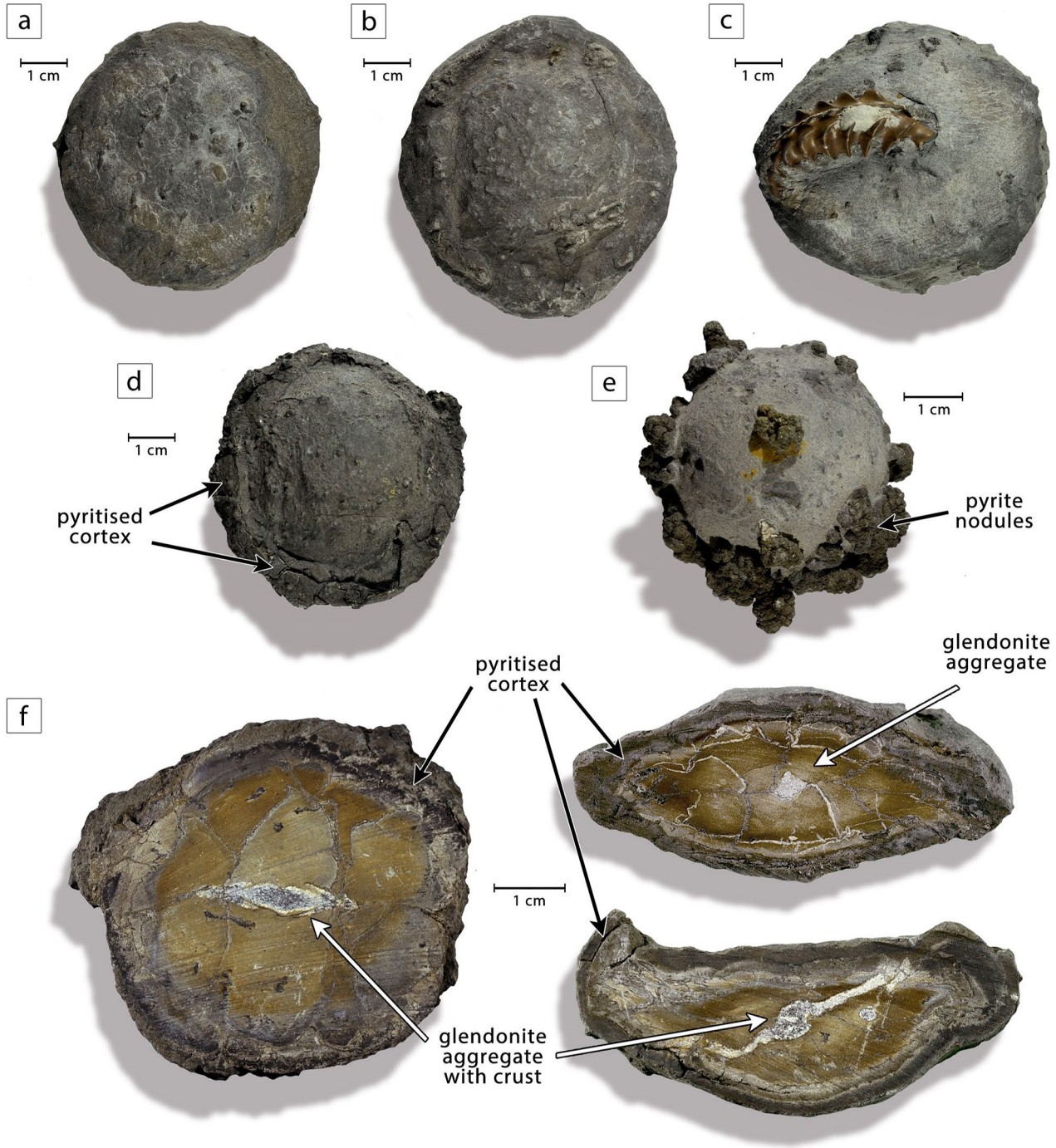

Fig. 5 Glendonite-bearing concretions ("discus concretions") recovered below the "Bollernbank" limestone bed. **a** Concretion with the typical discus shape and a smooth surface. **b** Concretion with the typical discus shape. **c** Concretion with a protruding *Pleuroceras* shell. **d** Discus-shaped concretion with a slightly weathered cortex consisting of pyritised material. **e** Spherical concretion with pyrite nodules on the smooth outer surface. **f** Slabbed discus concretions with glendonite aggregates in the centre and pyritised cortices

and Derkachev 2004; Teichert and Luppold 2013). Moreover, the favouring influence of methane has been discussed for recent ikaite occurrences (Schubert et al. 1997; Kodina et al. 2003; Krylov et al. 2015) as well as for examples from the fossil record (Teichert and Luppold 2013; Morales et al. 2017; van de Schootbrugge et al. 2019), since AOM facilitates the precipitation of authigenic carbonates.

The formation of carbonate minerals requires bicarbonate (HCO_3^-) which is available in the water column or can be released by specific chemical processes in the

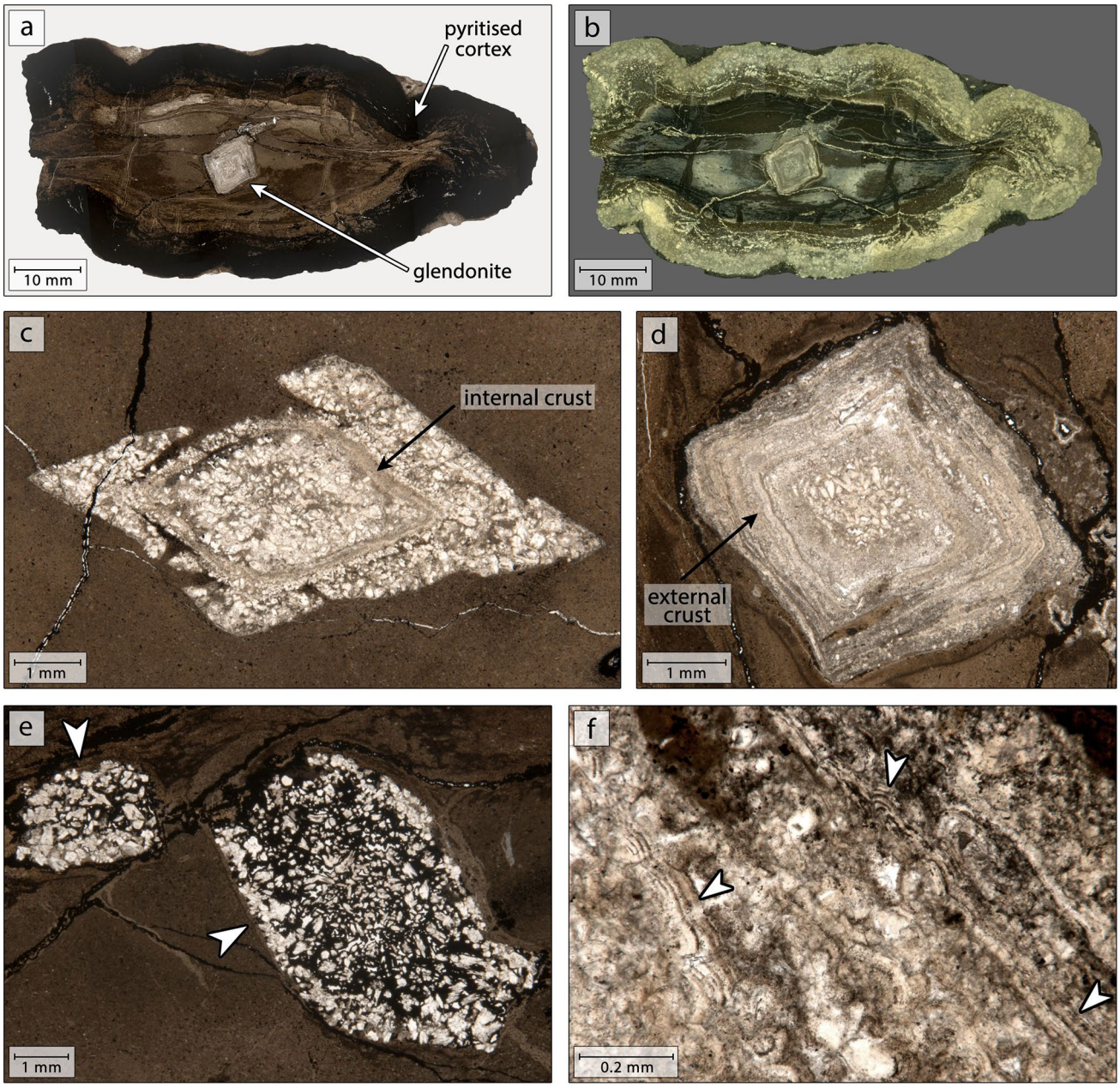

Fig. 6 Photomicrographs of glendonite-bearing concretions. **a** Transmitted light photomicrograph of a discus-shaped concretion; note the pyritised concretion margin and the rhombic glendonite crystal in the centre; thin section no. BU-G-20. **b** Reflected light photomicrograph of the same specimen shown in a. **c** Rhombic glendonite aggregate with an internal crust; thin section no. BU-G-17. **d** Rhombic glendonite aggregate with a thick, external crust consisting of multiple layers; thin section no. BU-G-20. **e** Glendonite aggregate with an irregular outline (arrows) and pore-filling pyrite in the aggregate centre; thin section no. BU-G-12. **f** Detail of a crust surrounding a glendonite aggregate; some layers show a zonation and a cauliflower-like growth (white arrows); thin section no. BU-G-20

shallow subsurface involving the oxidation of organic matter and/or methane. It is possible to distinguish different HCO_3^- sources by their carbon isotope signatures. In the Pliensbachian, inorganic carbon dissolved in seawater had typical $\delta^{13}C$ values between 0.0 and + 3.0‰ VPDB (Jenkyns et al. 2002). In pre-Paleogene times marine organic matter was enriched in ^{12}C compared to land plant organic matter (Arthur et al. 1985; Hayes et al. 1999). Typical carbon isotope signatures of marine organic matter in the Jurassic were − 26 to − 32‰ VPDB. Values ranging from − 20 to − 28‰ VPDB can be measured if larger amounts of terrestrial organic matter were present. Thermogenic methane shows carbon isotope values between − 50.0 and − 30.0‰ VPDB, and the isotopic signature of biogenic

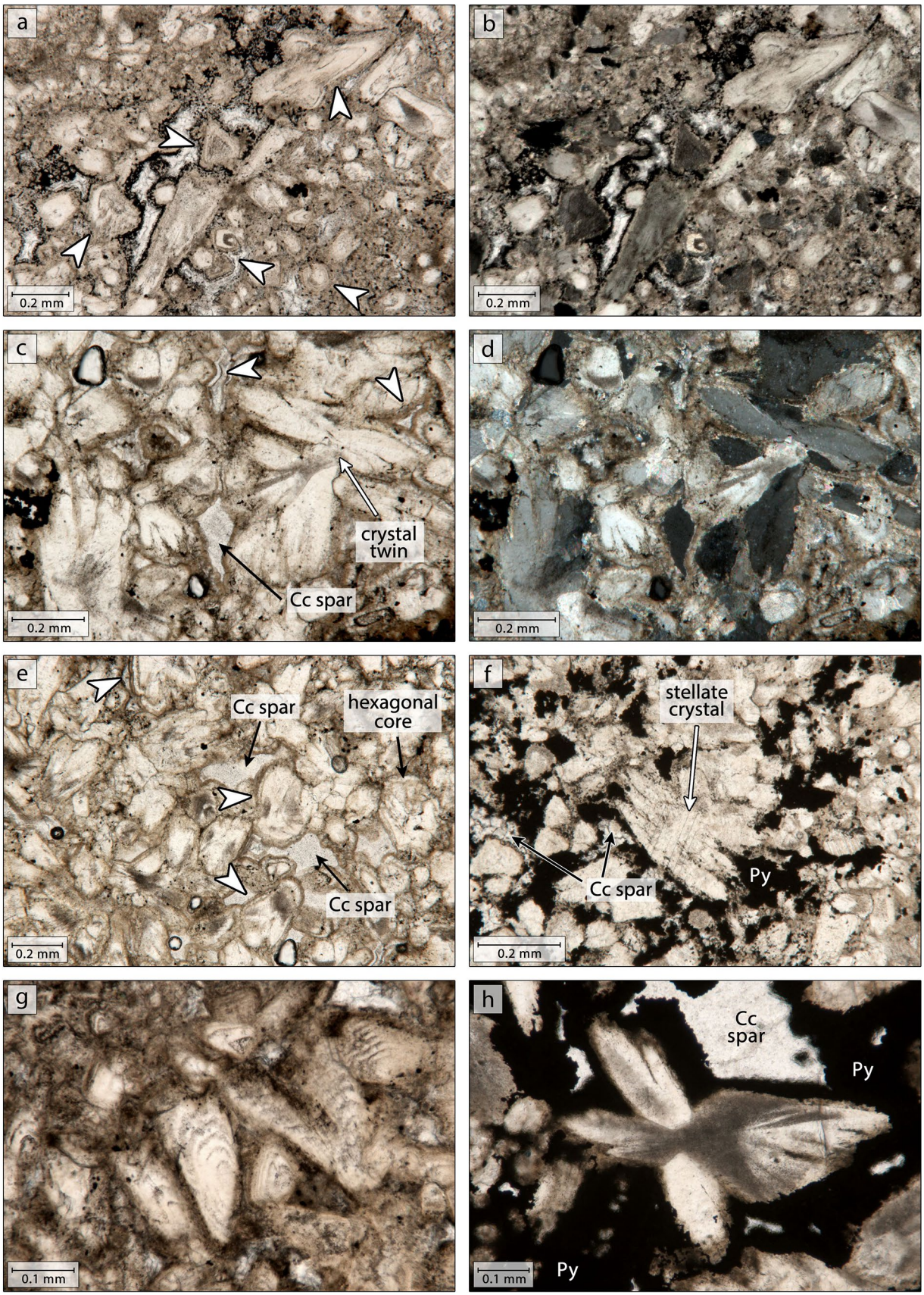
a
0.2 mm
b
0.2 mm
c
crystal twin
Cc spar
0.2 mm
d
0.2 mm
e
Cc spar
hexagonal core
Cc spar
0.2 mm
f
stellate crystal
Cc spar
Py
0.2 mm
g
0.1 mm
h
Cc spar
Py
Py
0.1 mm

◂**Fig. 7** Photomicrographs of the internal fabric present in the glendonite aggregates. **a** Microfabric typical for precursor ikaite (guttulatic microtexture); arrows indicate crystals consisting of a core and subsequent overgrowth by one or more calcite generation(s); thin section no. BU-G-19. **b** Same section as shown in a; note the syntaxial extinction behaviour of the cement overgrowth; crossed-polarised light. **c** Guttulatic microfabric with crystal twin; note the calcite cement overgrowing the crystal cores (white arrows); thin section no. M-BU-77b. **d** same section as shown in c, crossed-polarised light. **e** Guttulatic microfabric with pronounced calcite overgrowth surrounding the crystal cores (white arrows) which show various shapes (hexagonal, irregular, spherical); remaining pore space is filled with calcite spar; thin section no. M-BU-77b. **f** Photomicrograph of a stellate crystal; note the lack of clear cement rims around the crystals; pore space is filled with pyrite (py) or calcite spar; thin section no. M-BU-77b. **g** Calcite crystals with a distinct zonation; note the brownish rims surrounding the crystals; thin section no. BU-G-20. **h** Crystal twin overgrown by pyrite (py); note the absence of an overgrowth by clear calcite; instead, a thin brownish rim is visible; remaining pore space is filled with calcite spar; thin section no. BU-G-9

methane ranges from − 110.0 to − 50.0‰ VPDB (Whiticar 1999).

It should be noted that mixing of the mentioned bicarbonate sources can take place. Thus, it is difficult to make a clear statement about the absolute contributions of the different sources. Another important point is that the isotope values obtained from the studied glendonites represent the HCO_3^- composition of the fluid during the breakdown of the ikaite and the precipitation of the subsequent cement generations. However, the low variability in the elemental composition of the different calcite generations mentioned in the previous chapter suggests stable geochemical conditions in the subsurface and/or rapid cement growth. Moreover, the first calcite generation present in the glendonite paragenetic sequence precipitates directly from the fluids which were released during the decomposition of ikaite and therefore reflect the isotopic signatures of the precursor crystal (Selleck et al. 2007).

The $\delta^{13}C$ values of the Buttenheim glendonites range between − 21.8 and − 10.3‰ VPDB (Table 2, Fig. 8). This suggests that a mixture of inorganic HCO_3^- from seawater and bicarbonate from the decomposition of organic matter were involved in the formation of the glendonite. Since the studied site was located close to the Bohemian landmass, wood fragments and other plant remains are common in the outcrop suggesting that the organic matter was derived from both marine and terrestrial sources.

Minor contributions of HCO_3^- derived by AOM cannot be excluded, but it seems unlikely that methane played a prominent role, because otherwise more negative $\delta^{13}C$ values would be expected. Further evidence arguing against an influence of methane, especially methane derived by seepage, is provided by the fact that the glendonite-bearing concretions occur over the entire outcrop length in a thin layer and are not restricted to single patches as it would be the case if the glendonite occurrences were bound to methane seeps. This observation is in line with occurrence patterns reported for Siberian glendonites of the same age which can be traced over long distances and are therefore used as marker horizons (Rogov et al. 2023).

Comparison of the Buttenheim glendonites with other upper Pliensbachian occurrences

So far, upper Pliensbachian glendonites are known from Siberia and Northern Germany. Occurrences in Siberia are located around the Lena River region with a palaeolatitude ranging from 70° to 85° N (Fig. 1b) (e.g., Kaplan 1978; Suan et al. 2011; Nikitenko et al. 2013; Rogov 2015; Morales et al. 2017; Rogov et al. 2021, 2023). In Northern Germany, glendonites have been found in drill cores from Mecklenburg–Western Pomerania (near the town of Barth, Barth et al. 2018, and near the city of Schwerin, Zimmermann et al. 2015) and in drill cores and outcrops in Lower Saxony (near the city of Braunschweig, Teichert and Luppold 2013; van de Schootbrugge et al. 2019). This paper adds a new glendonite occurrence site to this list which is located in Bavaria (near the city of Bamberg). German sites have a palaeolatitude between 40° and 45° N (Fig. 1c). All mentioned glendonite occurrences are found in marine sequences consisting of clay-, marl- or siltstone and commonly contain carbonate concretions. In some cases, the glendonites are found inside such carbonate bodies. The pseudomorphs can reach different sizes ranging from a few millimetres to several centimetres. Moreover, the glendonites in the described sections are not randomly distributed but are restricted to discrete layers.

Only three of the above-mentioned studies of Pliensbachian glendonites contain isotopic data. Glendonites from Anabar Bay, Siberia, Russia, show a large scatter with $\delta^{13}C$ values ranging from − 37.3 to − 12.6‰ VPDB (Fig. 8) (Morales et al. 2017). Isotope values measured in glendonites recovered from an outcrop near Braunschweig, Northern Germany, range from − 45.0 to − 20.0‰ VPDB (Fig. 8) (Teichert and Luppold 2013). Van de Schootbrugge et al. (2019) reported glendonites and glendonite-bearing concretions from a drill core located close to the site described by Teichert and Luppold (2013). The glendonites analysed by van de Schootbrugge et al. (2019) also show very light $\delta^{13}C$ values between − 36.0 and − 20.0‰ VPDB (Fig. 8).

Considering the light carbon isotope signature of the measured glendonites all authors have concluded that bicarbonate derived by AOM played a dominant role in the formation of the precursor ikaite and suggested methane seepage as the source. Since the glendonite occurrences in Northern Germany are located in areas with a palaeolatitude

Table 2 Stable carbon and oxygen isotope data measured in glendonite-bearing concretions

Isotope sample no	Specimen no	Analysed material	$\delta^{13}C‰$ VPDB	$\delta^{18}O‰$ VPDB
1	Iso-G-1	Glendonite	− 10.98	− 6.51
2	Iso-G-2	Glendonite	− 18.18	− 4.41
3	Iso-G-3	Glendonite	− 12.22	− 6.61
4	Iso-G-4	Glendonite	− 17.76	− 5.86
5	Iso-G-5	Glendonite	− 14.99	− 9.45
6	Iso-G-6	Glendonite	− 17.44	− 5.43
7	Iso-G-7	Glendonite	− 13.51	− 6.34
8	Iso-G-8	Glendonite	− 17.54	− 4.32
9	Iso-G-9	Glendonite	− 10.34	− 7.08
10	Iso-G-10	Glendonite	− 14.07	− 6.56
11	Iso-G-11	Glendonite	− 16.59	− 4.80
12	Iso-G-12	Glendonite	− 14.5	− 6.01
13	Iso-G-13	Glendonite	− 14.75	− 6.03
14	Iso-G-14	Glendonite	− 14.93	− 7.09
15	Iso-G-15	Glendonite	− 17.47	− 4.95
16	Iso-G-16	Glendonite	− 16.88	− 4.82
17	Iso-G-17	Glendonite	− 21.82	− 3.62
18	Iso-G-18	Glendonite	− 16.33	− 4.80

corresponding approximately to the present-day latitude of northern Italy it seems that the climate conditions were too warm for the formation of ikaite. Therefore, Teichert and Luppold (2013) as well as van de Schootbrugge et al. (2019) assumed that the glendonite occurrences were directly linked to the presence of methane seeps which favoured the formation of precursor ikaite at temperatures slightly above its stability window.

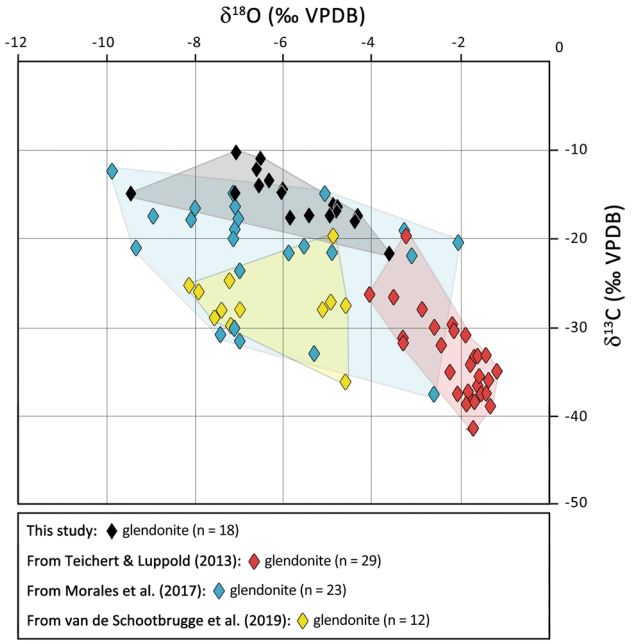

Fig. 8 Cross-plot of $\delta^{13}C$ and $\delta^{18}O$ values (both reported in ‰ VPDB) of glendonite aggregates from Buttenheim, S-Germany (this study), Cremlingen and Schandelah near Braunschweig, N-Germany (from Teichert and Luppold 2013; van de Schootbrugge et al. 2019) and Anabar Bay, W-Siberia (from Morales et al. 2017). Pale shaded fields indicate the value distribution of the glendonites

Significantly heavier carbon isotope values measured in glendonites from Buttenheim (Fig. 8) contradict an interpretation as a hydrocarbon seep. This is supported by the fact, that the glendonite-bearing concretions are restricted to a discrete layer of only a few centimetres thickness, but with at least several tens of metres lateral extent. Hydrocarbon seeps usually show a restricted extent and affect the entire sediment column and not only a single layer. The shape of the glendonite-bearing concretions argues in the same direction, since they have a flat, discus-like appearance (Figs. 2e, 5a–c, f) which suggests that the concretions formed in a very narrow layer in the shallow subsurface. Furthermore, the Buttenheim succession lacks sedimentological evidence for a seep such as crusts consisting of botryoidal cement bushes and tubular cements as well as a chemosynthetic fauna. Teichert and Luppold (2013) as well as van de Schootbrugge et al. (2019) noticed the absence of typical seep features in their study areas and concluded that the release of hydrocarbons took place in a very slow and diffuse way.

However, the presence of methane does not necessarily require seepage in a narrower sense. Methane is produced by methanogenesis in the sediment column below the zone of anaerobic oxidation of methane (Jørgensen and Kasten 2006). Carbonate precipitated in this particular zone therefore shows very light carbon isotope values which could

explain the values measured in the above-mentioned studies without hydrocarbon seepage. We therefore propose an alternative hypothesis for the formation of glendonite in the European epicontinental sea which will be elaborated in the following sections.

Intensity and extent of the late Pliensbachian cooling and its impact on the formation of cold bottom waters on the continental shelf

Despite ongoing research, the intensity of the late Pliensbachian cooling event is still debated, especially with regard to its impact on mid-latitudinal areas. Several palaeoecological studies on marine and terrestrial organisms as well as on land plants have yielded ambiguous results. For example, Mehlqvist et al. (2009) suggested a warm and humid climate with a pronounced seasonality typical for the warm temperate zone based on analyses of plant remains recovered from a late Pliensbachian delta complex located on the island of Bornholm, Denmark. However, several studies on the fossil record of marine invertebrates have revealed the presence of cold-water adapted taxa in the European Realm. Arp and Seppelt (2012) described the migration of *Palmoxytoma cygnipes* into the central part of the European epicontinental sea based on specimens found in northern Germany, France, England and Sweden (Fig. 1c). *P. cygnipes* is a bivalve species adapted to cool water temperatures and was also described in the Buttenheim clay pit by Schweigert (2019). In addition, Keupp (2021a) noticed a shift of foraminiferal assemblages dominated by calcitic taxa towards assemblages dominated by textulariid taxa (i.e., with agglutinated shells) in the upper *P. spinatum* Zone of the Buttenheim clay pit which is indicative of a decrease in water temperature.

As mentioned in the previous section, some glendonite occurrences in North Germany were interpreted as an indicator for methane seepage but not as one for low temperature. We disagree with this interpretation, since the studied material from South Germany lacks sedimentological and geochemical evidence for hydrocarbon seepage and suggests that a low temperature was the main factor controlling the formation of precursor ikaite. This is in line with previous investigations showing that recent ikaite exclusively occurs in cold environments, such as polar regions (e.g., Suess et al. 1982; Stein and Smith 1985; Greinert and Derkachev 2004; Dahl and Burchardt 2006), in deep sea fans (Zabel and Schulz 2001), in cool alkaline and saline lakes (Bischoff et al. 1993; Council and Bennett 1993; Last et al. 2013; Oehlerich et al. 2013; Scheller et al. 2022) and in cold caves (Chaikovskiy and Kadebskaya 2014; Bazarova et al. 2016). So far, no natural locality is known where ikaite formed at higher temperatures–even if the alkalinity and the phosphorus content are very high (Bischoff et al. 1993; Council and Bennett 1993). Moreover, ancient glendonite has never been observed in localities representing tropical or subtropical environments (Rogov et al. 2023). Therefore, it is assumed that the glendonites found in the Buttenheim clay pit represent former ikaite crystals that were formed due to cold water temperatures.

This raises the question as to which process could have facilitated the cooling of water masses in the European epicontinental sea during the late Pliensbachian. Taking modern analogues into account, it is conceivable that the configuration of marine currents played an important role.

A normal thermohaline circulation develops when cold, saline water sinks below a warmer water mass, forming a thermocline in between (Fig. 9a). Massive global cooling and the formation of polar ice caps influence this process. Nowadays, cold bottom waters form in high latitudes due to the cooling of warm, saline surface currents, which become increasingly heavy and sink downward as a result of cooling, e.g., in the northern North Atlantic (North Atlantic Deep Water, NADW; Dickson and Brown 1994). On the Antarctic shelf, however, another process is involved in the formation of cold bottom waters. Here, the formation of sea ice in autumn and winter produces very saline, heavy brines that sink to the bottom (Antarctic Bottom Water, AABW; Orsi et al. 1999). Moreover, coastal polynyas, which are ice-free zones between the ice sheet and the adjacent sea ice, intensify the heat loss (Ohshima et al. 2016).

Both possibilities could apply to the situation during the late Pliensbachian. Despite ongoing discussions, it is assumed by several authors that parts of the Arctic Realm were covered by ice sheets of debated extent at that time (Fig. 1b) (Donnadieu et al. 2011; Korte and Hesselbo 2011; Suan et al. 2011; Dera and Donnadieu 2012; Ruebsam et al. 2019; Nordt et al. 2021, Ruebsam and Schwark 2021). The occurrence of dropstones in late Pliensbachian sections located in high palaeolatitudes suggest a widespread formation of sea ice (Fig. 1b) (Suan et al. 2011; Ruebsam and Schwark 2021). The opening of the Viking Corridor in the Early Jurassic enabled a water mass exchange between the Arctic Realm in the north and the Tethyan Realm in the south (Fig. 1b, c) (Surlyk 2003; Korte et al. 2015). We therefore assume that very dense cold-water masses, which were formed due to the same processes responsible for the production of modern AABW and/or NADW, sank to the shelf floor, flowed southwards into the Tethys Ocean and resulted in a pronounced thermocline in vast areas of the European epicontinental sea (Fig. 9b). Such cold currents could have triggered the formation of ikaite in areas in which the mineral otherwise could not form.

It should be noted that this model does not necessarily require a large, permanent ice sheet. The proposed mechanisms were driven by a strong temperature gradient in high latitudes and the formation of sea ice in autumn and winter.

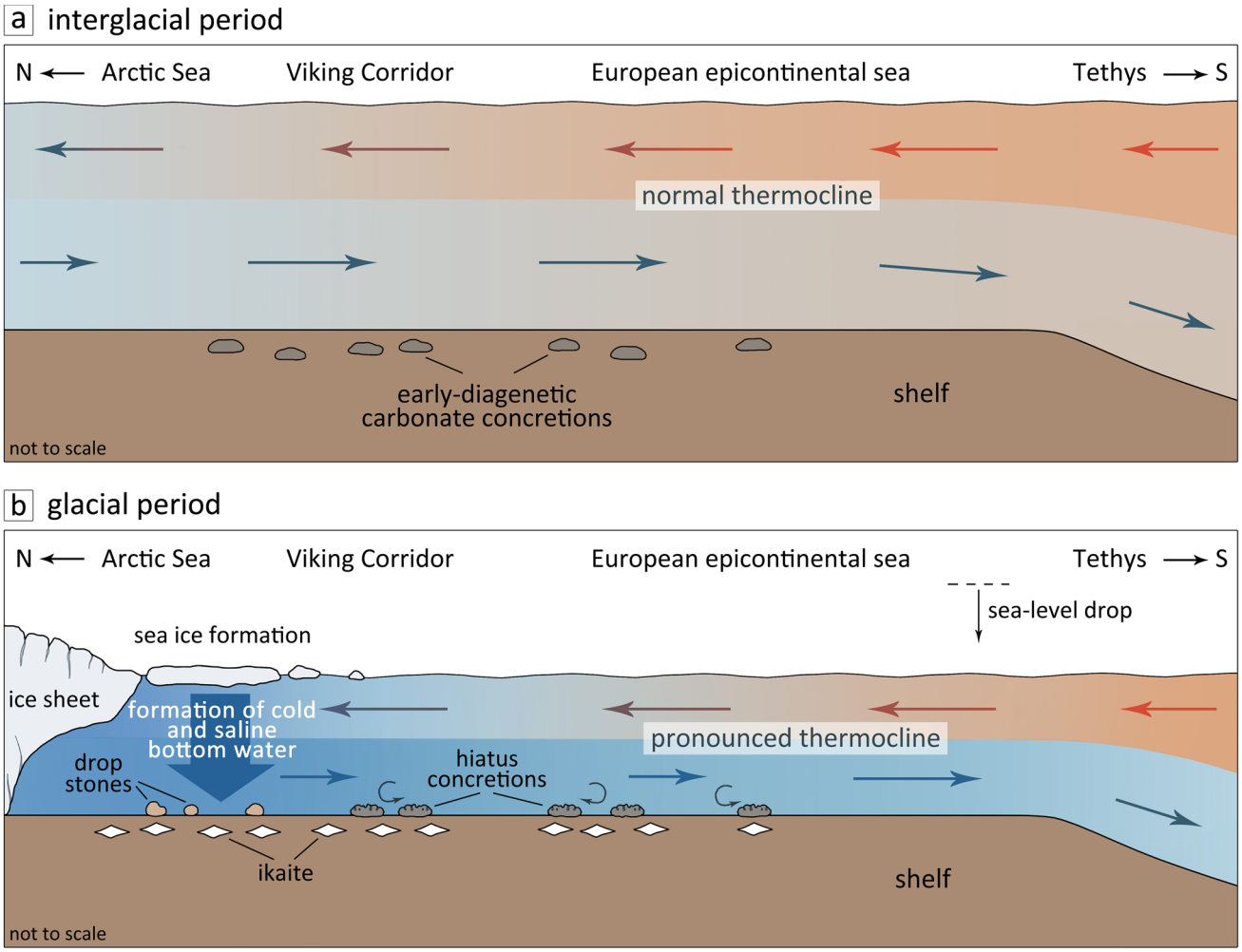

Fig. 9 Schematic drawing showing the formation of cold and dense bottom water. **a** Situation in the European epicontinental sea during an interglacial period with a sea-level highstand with early diagenetic carbonate concretions forming in the shallow subsurface. **b** Situation during a glacial period with the formation of very cold and dense bottom waters due to brine injection caused by the formation of sea ice; the cold bottom waters triggered the formation of ikaite in the sediment; during the sea-level lowstand, hiatus concretions were formed due to winnowing of the soft sediment

Both processes are independent of the dimension of the ice sheet.

This process probably affected large parts of the epeiric sea. It is therefore possible that glendonites or glendonite-bearing concretions occur in other late Pliensbachian localities throughout the European Realm beside the so-far known localities in Germany, but they have been overlooked so far, because glendonite aggregates can be very small (< 1 cm). Furthermore, they can have a rather inconspicuous appearance, especially if they are surrounded by carbonate concretions. In this case, the guttulatic microfabric, which is only visible in thin section, is the best criterion to identify the pseudomorph. Therefore, the spatial distribution of glendonite in the late Pliensbachian might be underestimated.

The presence of a pronounced thermocline with very cold bottom waters and overlying warmer surface waters can also offer an explanation for the ambiguous results of palaeoecological investigations on marine and terrestrial taxa. Warm-adapted organisms were restricted to the surface water and the emergent lands, whereas cold-adapted taxa colonised the lower part of the water column and the seafloor.

Hiatus concretions as witnesses of glacial sea-level falls

In the Buttenheim clay pit, the extensive bioerosion of the hiatus concretions suggests that the exhumation of the concretions could not have been due to a short-termed event, such as a hurricane or a tsunami, since a longer period of sediment starvation is required in the aftermath for successful colonisation by sessile organisms and microbes. The exhumation process requires an increase in

water energy, leading to the winnowing of the soft sediment cover. It can be assumed that the turbulent conditions persisted during the subsequent sedimentation gap as indicated by the enrichment of bioclasts in the sediment surrounding the hiatus concretions (Figs. 3c, 4c, e, f). Especially in the "Bollernbank" limestone bed, well-sorted bioclasts and the removal of fine-grained material point towards constant water movement (Fig. 4f, g). Moreover, the colonisation and bioerosion of hiatus concretions and belemnite rostrums commonly occur on all sides suggesting that the components were turned over frequently. This can be explained by intense water movement but also by the activity of foraging organisms.

An increase in water energy can occur either due to a change in bottom current energy or due to the lowering of the wave base (Sadlok and Zatoń 2020). The latter could be explained by a sea-level fall. The Pliensbachian–Toarcian transition is indeed characterised by a widespread hiatus which has been interpreted as the result of a glacially induced sea-level fall (Morard et al. 2003; Haq 2018; Ruebsam and Al-Husseini 2020; Bodin et al. 2023). This corresponds with the occurrence of hiatus concretions and other reworked components in the "Bollernbank" limestone bed in Buttenheim which forms the most pronounced reworked interval in the studied succession. The glendonite-bearing layer is located right below this interval (Fig. 2b, c), indicating a formation of precursor ikaite within the sediment during the sea-level lowstand, thereby linking the sedimentological evidence for a sea-level fall, i.e., the hiatus, to a mineralogical indication for a cold climate, i.e., the occurrence of glendonite (Fig. 9b).

Following this interpretation, we propose a similar cause for the formation of the other hiatus concretion-bearing intervals in Buttenheim ("Pyriterzbank", "Quellhorizont", and "Echiniden-Pectiniden-Horizont", Fig. 2b). The hiatuses probably represent recurrent glacial pulses during the overall cool climate in the late Pliensbachian, producing brief sea-level falls (Fig. 10). This assumption is supported by the occurrence of quartz-rich sediments surrounding the hiatus concretions of the "Quellhorizont" reworked interval (Munnecke and Merkel 2021) and the "Echiniden-Pectiniden-Horizont" interval in Buttenheim (Keupp 2021d). This finding indicates a temporarily enhanced siliciclastic input caused by a basin-ward movement of river mouths during the sea-level lowstand. In accordance, Barth et al. (2018) pointed out that a rapid shoreline shift was observed in upper Pliensbachian deposits from northern Germany and Poland, representing a near-shore facies. Since the authors also report glendonites in the studied boreholes, they suggest recurrent glaciations and deglaciations as the driving mechanism for the short-term sea-level fluctuations. However, the extent to which the proposed sea-level falls prior to the hiatus at the Pliensbachian–Toarcian boundary can be correlated with other late Pliensbachian successions must be examined by further research.

So far, no glendonites have been found in the Buttenheim clay pit that were associated with the "Pyriterzbank", "Quellhorizont", or "Echiniden-Pectiniden-Horizont" intervals. This could either mean that they simply have not been discovered yet or that the glacial pulses causing the sea-level falls were less intense than the one responsible for the formation of the "Bollernbank" limestone bed and the associated glendonite-bearing concretions at the Pliensbachian–Toarcian boundary. Field observations support the latter assumption, since the reworked intervals in the Buttenheim section become more pronounced with increasing stratigraphic height as indicated by a stronger colonisation and bioerosion of components and an increasing thickness of the bioclast-rich sediment surrounding the hiatus concretions. A similar trend can be observed in the foraminifera assemblage: agglutinating taxa associated with a cooler water temperature become more abundant in the upper *P. spinatum* Zone (Keupp 2021a). This means, in summary, that the "Pyriterzbank" reworked interval represents the weakest glacial pulse in the *P. spinatum* Zone, whereas the "Bollernbank" limestone bed was caused by the most intense cold snap (Fig. 10). It is interesting to note that some late Pliensbachian successions in Siberia (Vilyui river area) show a similar tendency regarding the size of glendonites recovered from these sections. The oldest specimens are rather small compared to those occurring close to the Pliensbachian–Toarcian boundary (Rogov et al. 2023). This observation supports the hypothesis of recurrent glaciations with increasing intensity.

Conclusions about the amplitude of the proposed sea-level falls cannot be drawn based on the data acquired in this study. However, studies on the Pliensbachian–Toarcian boundary hiatus have concluded that the associated sea-level fall probably had an amplitude of 50–70 m (Marjanac and Steele 1997; Ruebsam et al. 2020).

The deposits located between the "Pyriterzbank", the "Quellhorizont" and the "Echiniden-Pectiniden-Horizont" reworked intervals are characterised by mass occurrences of ammonite shells which are interpreted as the result of condensation due to sea-level highstands (Keupp 2021d). This suggests that the glacial pulses were interrupted by short phases of moderate warming causing a decline of polar ice sheets which could have led to brief sea-level rises (Fig. 10) and a reduction in cold bottom water formation (Fig. 9a). Such an alternation of glacial pulses of variable intensity and intermediate phases of moderate warming would explain the partly contrary results of studies dealing with faunal and floral assemblages in the European Realm in addition to the thermohaline circulation. However, since the glacial phases are mainly characterized by erosion, there is hardly any fossil evidence for the cold periods, except for the bioclastic-rich

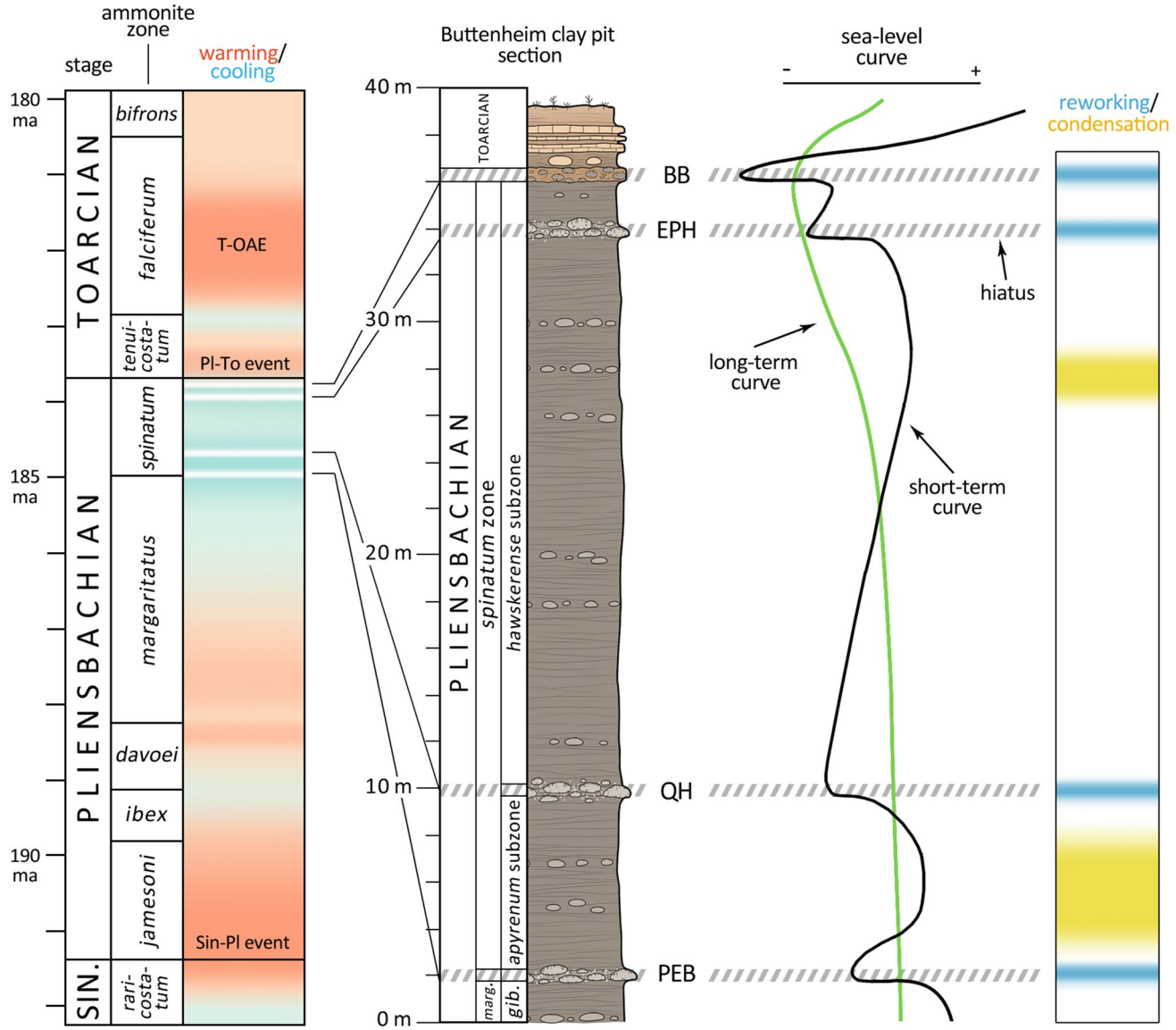

Fig. 10 Correlation between the occurrence of reworked intervals in the Buttenheim clay pit with the fluctuating climate in the Early Jurassic. Right: recurrent warming and cooling in the Early Jurassic (climate data compiled from Suan et al. 2010; Korte and Hesselbo 2011; Bodin et al. 2016; Bougeault et al. 2017; Krencker et al. 2019; Ruebsam et al. 2020; Schöllhorn et al. 2020a, b; Peti and Thibault 2022; ages and duration of ammonite zones are taken from Haq 2018); left: section of the Buttenheim clay pit with the so far known reworked intervals (BB = "Bollernbank" limestone bed; EPH = "Echininden-Pectiniden-Horizont"; PEB = "Pyriterzbank"; QH = "Quellhorizont"); short-term sea-level curve shows assumed sea-level falls driven by recurrent glacial pulses correlating with reworked intervals; intervals characterised by condensation are caused by sea-level highstands during interglacial periods; long-term sea-level curve shows the overall regressive trend in the late Pliensbachian

layers around the hiatus concretions and the incrusting and bioeroding organisms.

Conclusions

Different types of carbonate concretions exposed in the upper Pliensbachian succession of Buttenheim, South Germany, were analysed by optical and geochemical methods to shed light on the climatic conditions prevailing at the time of deposition.

The petrographic analysis reveals that discus-shaped concretions occurring in a distinct layer ca. 30 cm below the Pliensbachian–Toarcian transition contain millimetre-sized glendonite aggregates which are pseudomorphs after the cryophilic mineral ikaite. This finding represents the southernmost occurrence of glendonite in the late Pliensbachian so far discovered. The aggregates consist of granular calcite

crystals overgrown by a (syntaxial) cement generation and pore-filling calcite or pyrite, forming a so-called guttulatic microfabric which is diagnostic of the precursor ikaite. Stable carbon isotope values between − 21.8 and − 10.3‰ VPDB suggest that HCO_3^- derived by the decay of organic matter was the main carbonate source during the ikaite formation. Contributions of carbonate derived by AOM were considered as insignificant. It is therefore concluded that the formation of the Buttenheim ikaites/glendonites was not triggered by the release of methane due to hydrocarbon seepage which has been proposed to facilitate the precipitation of authigenic carbonate minerals, such as ikaite. Instead, the glendonites are interpreted as indicators of very low bottom water temperatures, supporting the hypothesis of a massive cooling during the late Pliensbachian which even impacted mid-latitude realms. To explain this, it is proposed that cold and dense bottom waters were formed in the Arctic Realm which then flowed southward into the European epicontinental sea, forming a pronounced thermocline and enabling the precipitation of ikaite in the sediment.

Further sedimentological evidence for cooling is provided by the occurrence of recurrent reworked intervals in the studied section of which one is associated with the glendonite-bearing concretions close to the Pliensbachian–Toarcian boundary. It is therefore proposed that the reworked intervals formed due to glacially induced sea-level falls. This means that the overall cool climate in the late Pliensbachian was characterised by at least four distinct glacial pulses.

Acknowledgements The authors would like to thank Johann Schobert (Hirschaid) for his tireless support during the field work and the collection of additional sample material. Thanks are also due to Liapor GmbH & Co. KG (Hallerndorf) for giving access to their facilities. Birgit Leipner-Mata (Erlangen) is thanked for excellent thin section preparation as well as Christian Schulbert (Erlangen) for the support during the EDX analysis. Michael Joachimski (Erlangen) and Daniele Lutz (Erlangen) are thanked for the stable isotope analyses. The authors are very grateful to Mikhail Rogov (Moscow) for improving the manuscript with helpful comments. This work also benefited from comments and suggestions made by an anonymous reviewer as well as by the editor Maurice Tucker.

Funding Open Access funding enabled and organized by Projekt DEAL.

Data availability The authors declare that the data supporting the findings of this study are available within the paper.

Declarations

Conflict of interest The authors have no competing interests to declare that are relevant to the content of the article and did not receive support from any organization for the submitted work.

References

Arp G, Seppelt S (2012) The bipolar bivalve *Oxytoma* (*Palmoxytoma*) *cygnipes* (Young & Bird, 1822) in the Upper Pliensbachian of Germany. Paläontologische Z 86(1):43–57. https://doi.org/10.1007/s12542-011-0113-1

Arthur MA, Dean WE, Claypool GE (1985) Anomalous ^{13}C enrichment in modern marine organic carbon. Nature 315:216–218. https://doi.org/10.1038/315216a0

Barth B, Pieńkowski G, Zimmermann J, Franz M, Kuhlmann G (2018) Palaeogeographical evolution of the Lower Jurassic: high-resolution biostratigraphy and sequence stratigraphy in the Central European Basin. Geol Soc Spec Publ 469:341–369. https://doi.org/10.1144/SP469.8

Bazarova E, Kononov A, Gutareva O (2016) Cryogenic mineral formations in the Okhotnichya Cave in the Primorsky Mountain Ridge (western Baikal Region, Russia). Eurospeleo Mag 3:47–59

Bischoff JL, Stine S, Rosenbauer RJ, Fitzpatrick JA, Stafford TW (1993) Ikaite precipitation by mixing of shoreline springs and lake water, Mono Lake, California, USA. Geochim Cosmochim Acta 57:3855–3865. https://doi.org/10.1016/0016-7037(93)90339-X

Blakey RC (2016) Global Jurassic Paleogeographic Map (180MaBP): Molleweide. Global Paleogeography and Tectonics in Deep Time © 2016 Colorado Plateau Geosystems Inc. https://deeptimemaps.com. Accessed 15 May 2023.

Bodin S, Krencker F-N, Kothe T, Hoffmann R, Mattioli E, Heimhofer U, Kabiri L (2016) Perturbation of the carbon cycle during the late Pliensbachian–early Toarcian: new insight from high-resolution carbon isotope records in Morocco. J Afr Earth Sci 116:89–104. https://doi.org/10.1016/j.jafrearsci.2015.12.018

Bodin S, Fantasia A, Krencker F-N, Nebsbjerg B, Christiansen L, Andrieu S (2023) More gaps than record! A new look at the Pliensbachian/Toarcian boundary event guided by coupled chemo-sequence stratigraphy. Palaeogeogr Palaeoclimatol Palaeoecol 610:111344. https://doi.org/10.1016/j.palaeo.2022.111344

Boggs S Jr (1972) Petrography and geochemistry of rhombic, calcite pseudomorphs from mid-Tertiary Mudstones of the Pacific Northwest USA. Sedimentology 19(3–4):219–235. https://doi.org/10.1111/j.1365-3091.1972.tb00022.x

Bougeault C, Pellenard P, Deconinck J-F, Hesselbo SP, Dommergues J-L, Bruneau L, Cocquerez T, Laffont R, Huret E, Thibault N (2017) Climatic and palaeoceanographic changes during the Pliensbachian (Early Jurassic) inferred from clay mineralogy and stable isotope (C–O) geochemistry (NW Europe). Glob Planet Change 149:139–152. https://doi.org/10.1016/j.gloplacha.2017.01.005

Chaikovskiy II, Kadebskaya OI (2014) Mineral bodies of the Eranka cave in the Northern Urals. Probl Mineral Petrogr Metal 17:92–107

Clarkson JR, Price TJ, Adams CJ (1992) Role of metastable phases in the spontaneous precipitation of calcium carbonate. J Chem Soc Faraday Trans 88:243–249

Council TC, Bennett PC (1993) Geochemistry of ikaite formation at Mono Lake, California: implications for the origin of tufa

mounds. Geology 21:971–974. https://doi.org/10.1130/0091-7613(1993)021%3c0971:GOIFAM%3e2.3.CO;2
Dahl K, Buchardt B (2006) Monohydrocalcite in the arctic Ikka fjord, SW Greenland: first reported marine occurrence. J Sediment Res 76(3):460–471. https://doi.org/10.2110/jsr.2006.035
De Lurio JL, Frakes LA (1999) Glendonites as a paleoenvironmental tool: implications for early Cretaceous high latitude climates in Australia. Geochim Cosmochim Acta 63:1039–1048. https://doi.org/10.1016/S0016-7037(99)00019-8
Dera G, Donnadieu Y (2012) Modeling evidences for global warming, Arctic seawater freshening, and sluggish oceanic circulation during the early Toarcian anoxic event. Paleoceanography 27(2):PA2211. https://doi.org/10.1029/2012PA002283
Dera G, Pucéat E, Pellenard P, Neige P, Delsate D, Joachimski MM, Reisberg L, Martinez M (2009) Water mass exchange and variations in seawater temperature in the NW Tethys during the Early Jurassic: evidence from neodymium and oxygen isotopes of fish teeth and belemnites. Earth Planet Sci Lett 286:198–207. https://doi.org/10.1016/j.epsl.2009.06.027
Dera G, Brigaud B, Monna F, Laffont R, Pucéat E, Deconinck J-F, Pellenard P, Joachimski MM, Durlet C (2011) Climatic ups and downs in a disturbed Jurassic world. Geology 39(3):215–218. https://doi.org/10.1130/G31579.1
Dickson RR, Brown J (1994) The production of North Atlantic deep water: sources, rates and pathways. J Geophys Res 99:12319–12341
Dieckmann GS, Nehrke G, Papadimiriou S, Göttlicher J, Steininger R, Kennedy H, Wolf-Gladrow D, Thomas DN (2008) Calcium carbonate as ikaite crystals in Antarctic sea ice. Geophys Res Lett 35:L08501. https://doi.org/10.1029/2008GL033540
Donnadieu Y, Dromart G, Goddéris Y, Pucéat E, Brigaud B, Dera G, Dumas C, Olivier N (2011) A mechanism for brief glacial episodes in the Mesozoic greenhouse. Paleoceanography 26(3):PA3212. https://doi.org/10.1029/2010PA002100
Field LP, Milodowski AE, Shaw RP, Stevens LA, Hall MR, Kilpatrick A, Gunn J, Kemp SJ, Ellis MA (2017) Unusual morphologies and the occurrence of pseudomorphs after ikaite ($CaCO_3{\cdot}6H_2O$) in fast growing, hyperalkaline speleothems. Mineral Mag 81:565–589. https://doi.org/10.1180/minmag.2016.080.111
Frakes LA, Francis JE, Syktus JI (1992) Climate modes of the phanerozoic. Cambridge University Press, Cambridge
Gómez JJ, Comas-Rengifo MJ, Goy A (2016) Palaeoclimatic oscillations in the Pliensbachian (Early Jurassic) of the Asturian Basin (Northern Spain). Clim past 12(5):1199–1214. https://doi.org/10.5194/cp-12-1199-2016
Greinert J, Derkachev A (2004) Glendonites and methane-derived Mg-calcites in the Sea of Okhotsk, Eastern Siberia: implications of a venting-related ikaite/glendonite formation. Mar Geol 204:129–144. https://doi.org/10.1016/S0025-3227(03)00354-2
Haq BU (2018) Jurassic sea level variations: a reappraisal. GSA Today 28:4–10. https://doi.org/10.1130/GSATG359A.1
Hayes JM, Strauss H, Kaufman AJ (1999) The abundance of ^{13}C in marine organic matter and isotopic fractionation in the global biogeochemical cycle of carbon during the past 800 Ma. Chem Geol 161(103):125. https://doi.org/10.1016/S0009-2541(99)00083-2
Hollaar TP, Hesselbo SP, Deconinck J-F, Damaschke M, Ullmann CV, Jiang M, Belcher CM (2022) Environmental changes during the onset of the Late Pliensbachian event (Early Jurassic) in the Mochras Borehole, Cardigan Bay Basin, NW Wales. Clim past Discuss. https://doi.org/10.5194/cp-2022-87
Hu Y-B, Wang F (2020) Effect of ikaite precipitation on phosphate removal in sea ice. Polar Res 39:3413. https://doi.org/10.33265/polar.v39.3413
Hu Y-B, Dieckmann GS, Wolf-Gladrow DA, Nehrke G (2014) Laboratory study on coprecipitation of phosphate with ikaite in sea ice. J Geophys Oceans 119:7007–7015. https://doi.org/10.1002/2014JC010079
Huggett JM, Schultz BP, Smhearman DJ, Smith AJ (2005) The petrology of ikaite pseudomorphs and their diagenesis. Proc Geol Assoc 116:207–220. https://doi.org/10.1016/S0016-7878(05)80042-2
Ilyina VI (1969) The climate of Western and Middle Siberia in the early Jurassic epoch based on the palynological data. Geol Geofiz 10:10–17
Jenkyns HC (1988) The early Toarcian (Jurassic) anoxic event: stratigraphic, sedimentary, and geochemical evidence. Am J Sci 288:101–151. https://doi.org/10.2475/ajs.288.2.101
Jenkyns HC (2010) Geochemistry of oceanic anoxic events. Geochem Geophys Geosystems 11:1–30. https://doi.org/10.1029/2009GC002788
Jenkyns HC, Jones CE, Gröcke DR, Hesselbo SP, Parkinson DN (2002) Chemostratigraphy of the Jurassic system: applications, limitations and implications for palaeoceanography. J Geol Soc Lond 159:351–378. https://doi.org/10.1144/0016-764901-130
Jørgensen BB, Kasten S (2006) Sulfur cycling and methane oxidation. In: Schulz HD, Zabel M (eds) Marine geochemistry, 2nd edn. Springer, Heidelberg, pp 271–309. https://doi.org/10.1007/3-540-32144-6_8
Kaplan ME (1978) Calcite pseudomorphoses in Jurassic and lower Cretaceous deposits of the northern area of Eastern Siberia. Sov Geol Geophys 19(12):49–56
Kaplan ME (1980) Calcite pseudomorphs (pseudogaylussite, jarrowite, thinolite, glendonite, gennoishi, White Sea hornlets) in sedimentary rocks: origins of the pseudomorph. Lithol Miner Resour 14:623–636
Karapunar B, Werner W, Fürsich FT, Nützel A (2020) Taxonomy and palaeoecology of the Early Jurassic (Pliensbachian) bivalves from Buttenheim, Franconia (Southern Germany). Palaeontogr A (paleozool Stratigr) 318(1–4):1–127. https://doi.org/10.1127/pala/2020/0098
Keupp H (2021a) Lebewelt Im Verborgenen. Foss Spec 2021:15–20
Keupp H (2021b) Fische aus dem Amaltheenton. Foss Spec 2021:78–80
Keupp H (2021c) Die Hartgrund-Vergesellschaftung des „Echiniden-Pectiniden-Horizonts“. Foss Spec 2021:81–91
Keupp H (2021d) Die Tongrube am Holzbachacker südlich Buttenheim. Foss Spec 2021:4–14
Keupp H, Doppelstein B (2018) Foraminiferen und Rhabdopleuriden im Amaltheenton von Buttenheim. Fossilien 4:30–38
Keupp H, Fuchs D (2020) Enigmabelus n. Gen. (enigmabelitidae n.f.), an Early Jurassic (Late Pliensbachian) belemnite with an outstanding rostrum morphology. Neues Jahrb Für Geol Palaontol Abh 298(1):55–66. https://doi.org/10.1127/njgpa/2020/0933
Keupp H, Schobert J (2015) Schichtlücken im Amaltheenton von Buttenheim (Oberfranken). Fossilien 32(1):22–27
Keupp H, Schweigert G (2017) Exotische Kopffüßer im Amaltheentonvon Buttenheim. Fossilien 2017(6):54–58
Keupp H, Schweigert G (2021) Die Krebse (Crustacea) aus dem Amaltheenton von Buttenheim. Fossilien Spec 2021:59–66
Keupp H, Schobert J, Doppelstein B (2018) Treibgut im Fränkischen Amaltheenton. Fossilien 2018(5):34–39
Kodina LA, Tokarev VG, Vlasova LN, Korobeinik GS (2003) Contribution of biogenic methane to ikaite formation in the Kara Sea: evidence from the stable carbon isotope geochemistry. In: Stein R, Fahl K, Fütterer DK, Galimov EM, Stepanets OV (eds) Siberian River run-off in the Kara Sea: characterisation, quantification, variability, and environmental significance. Proceedings in marine sciences, vol 6. Elsevier, Amsterdam, pp 349–374. https://doi.org/10.1016/S1568-2692(03)80045-1
Korte C, Hesselbo SP (2011) Shallow marine carbon and oxygen isotope and elemental records indicate icehouse-greenhouse cycles

during the Early Jurassic. Paleoceanography 26(4):4219–4137. https://doi.org/10.1029/2011PA002160
Korte C, Hesselbo SP, Ullmann CV, Dietl G, Ruhl M, Schweigert G, Thibault N (2015) Jurassic climate mode governed by ocean gateway. Nat Commun 6:10015. https://doi.org/10.1038/ncomms10015
Krencker F-N, Lindström S, Bodin S (2019) A major sea-level drop briefly precedes the Toarcian oceanic anoxic event: implication for Early Jurassic climate and carbon cycle. Sci Rep 9:12518. https://doi.org/10.1038/s41598-019-48956-x
Krencker F-N, Fantasia A, Danisch J, Martindale R, Kabiri L, El Ouali M, Bodin S (2020) Two-phased collapse of the shallow-water carbonate factory during the late Pliensbachian–Toarcian driven by changing climate and enhanced continental weathering in the Northwestern Gondwana Margin. Earth Sci Rev 208:103254. https://doi.org/10.1016/j.earscirev.2020.103254
Krylov AA, Logvina EA, Matveeva TM, Prasolov EM, Sapega VF, Demidova AL, Radchenko MS (2015) Ikaite ($CaCO_3$*$6H_2O$) in bottom sediments of the Laptev Sea and the role of anaerobic methane oxidation in this mineral-forming process. Proc Russ Mineral Soc 4:61–75
Kutscher M, Reich M (2021) Die Echinodermen-Fauna des Amaltheentons von Buttenheim. Foss Spec 2021:67–77
Larsen D (1994) Origin and paleoenvironmental significance of calcite pseudomorphs after ikaite in the Oligocene Creede Formation, Colorado. J Sediment Res 64:593–603. https://doi.org/10.1306/D4267E1A-2B26-11D7-8648000102C1865D
Last FM, Last WM, Fayek M, Halden NM (2013) Occurrence and significance of a cold-water carbonate pseudomorph in microbialites from a saline lake. J Paleolimnol 50(4):505–517. https://doi.org/10.1007/s10933-013-9742-6
Marjanac T, Steele RJ (1997) Dunlin Group sequence stratigraphy in the Northern North Sea: a model for cook sandstone deposition. AAPG Bull 81:276–292. https://doi.org/10.1306/522B4307-1727-11D7-8645000102C1865D
Marland G (1975) The stability of $CaCO_3$*$6H_2O$ (ikaite). Geochim Cosmochim Acta 39:83–91. https://doi.org/10.1016/0016-7037(75)90186-6
McLachlan IR, Tsikos H, Cairncross B (2001) Glendonites (pseudomorphs after ikaite) in late Carboniferous Marine Dwyka beds in Southern Africa. South Afr J Geol 104:265–272. https://doi.org/10.2113/1040265
Mehlqvist K, Vajda V, Larsson LM (2009) A Jurassic (Pliensbachian) flora from Bornholm, Denmark—a study of a historic plant-fossil collection at Lund University, Sweden. GFF 131(1–2):137–146. https://doi.org/10.1080/11035890902975275
Meyer RKF, Schmidt-Kaler H (1992) Wanderungen in die Erdgeschichte (5): Durch die Fränkische Schweiz. Verlag Dr. Friedrich Pfeil, München
Mikhailova K, Rogov MA, Ershova V, Vereshchagin O, Shurekova O, Feodorova A, Zakharov V (2021) Middle Jurassic–Lower Cretaceous glendonites from the eastern Barents Shelf as a tool for paleoenvironmental and paleoclimatic reconstructions. Palaeogeogr Palaeoclimatol Palaeoecol 579:110600. https://doi.org/10.1016/j.palaeo.2021.110600
Morales C, Rogov M, Wierzbowski H, Ershova V, Suan G, Adatte T, Föllmi KB, Tegelaar E, Reichart G-J, de Lange GJ, Middelburg JJ, van de Schootbrugge B (2017) Glendonites track methane seepage in Mesozoic polar seas. Geology 45(6):503–506. https://doi.org/10.1130/G38967.1
Morard A, Guex J, Bartolini A, Morettini E, De Wever P (2003) A new scenario for the Domerian–Toarcian transition. Bull Soc Geol Fr 174(4):351–356. https://doi.org/10.2113/174.4.351
Müller T, Price GD, Bajnai D, Nyerges A, Kesjár D, Raucsik B, Varga A, Judik K, Fekete J, May Z, Pálfy J (2017) New multiproxy record of the Jenkyns Event (also known as the Toarcian Oceanic Anoxic Event) from the Mecsek Mountains (Hungary): differences, duration and drivers. Sedimentology 64(1):66–86. https://doi.org/10.1111/sed.12332
Munnecke A, Merkel A (2021) Mikrofazies der Hiatuskonkretionen im Amaltheenton von Buttenheim. Fossilien 6:36–51
Muramiya Y, Yoshida H, Minami M, Mikami T, Kobayashi T, Sekiuchi T, Katsuta N (2022) Glendonite concretion formation due to dead organism decomposition. Sediment Geol 429:106075. https://doi.org/10.1016/j.sedgeo.2021.106075
Nikitenko BL, Shurygin BN, Knyazev VG, Meledina SV, Dzyuba OS, Lebedeva NK, Peshchevitskaya EB, Glinskikh LA, Goryacheva AA, Khafaeva SN (2013) Jurassic and Cretaceous stratigraphy of the Anabar area (Arctic Siberia, Laptev Sea coast) and the Boreal zonal standard. Russ Geol Geophys 54:808–837. https://doi.org/10.1016/j.rgg.2013.07.005
Nordt L, Breecker D, White J (2021) Jurassic greenhouse ice-sheet fluctuations sensitive to atmospheric CO_2 dynamics. Nat Geosci 15:54–59. https://doi.org/10.1038/s41561-021-00858-2
Nützel A (2007) Leben am Meeresboden—Über die Fauna des fränkischen Amaltheentons. Jahresberichte und Mitteilung der Freunde der Bayerischen Staatssammlung für Paläontologie und Historische Geologie München e.V. 36:42–61
Nützel A, Gründel J (2015) Early Jurassic (Pliensbachian) gastropods from Franconia, Southern Germany. Palaeontogr A (paleozool Stratigr) 305(1–3):1–87. https://doi.org/10.1127/pala/305/2015/1
Oehlerich M, Mayr C, Griesshaber E, Lücke A, Oeckler OM, Ohlendorf C, Schmahl WW, Zolitschka B (2013) Ikaite precipitation in a lacustrine environment—implications for palaeoclimatic studies using carbonates from Laguna Potrok Aike (Patagonia, Argentina). Quat Sci Rev 71:46–53. https://doi.org/10.1016/j.quascirev.2012.05.024
Ohshima KI, Nihashi S, Iwamoto K (2016) Global view of sea-ice production in polynyas and its linkage to dense/bottom water formation. Geosci Lett 3:13. https://doi.org/10.1186/s40562-016-0045-4
Orsi AH, Johnson GC, Bullister JL (1999) Circulation, mixing, and production of Antarctic Bottom Water. Prog Oceanogr 43:55–109. https://doi.org/10.1016/S0079-6611(99)00004-X
Peti L, Thibault N (2022) Early Jurassic coccolith diversification and response to pre-Toarcian environmental changes: a perspective from the Paris Basin. Mar Micropaleontol 177:102173. https://doi.org/10.1016/j.marmicro.2022.102173
Price GD (1999) The evidence and implications of polar ice during the Mesozoic. Earth Sci Rev 48(3):183–210. https://doi.org/10.1016/S0012-8252(99)00048-3
Purgstaller B, Dietzel M, Baldermann A, Mavromatis V (2017) Control of temperature and aqueous Mg^{2+}/Ca^{2+} ratio on the (trans-) formation of ikaite. Geochim Cosmochim Acta 217:128–143. https://doi.org/10.1016/j.gca.2017.08.016
Richter AE (1985) Geologie und Paläontologie: Das Mesozoikum der Frankenalb—vom Ries bis ins Coburger Land. Franckh, Stuttgart
Rodríguez-Ruiz I, Veesler S, Gomez-Morales J, Delgado-Lopez JM, Grauby O, Hammadi Z, Candoni N, Garcia-Ruiz JM (2014) Transient calcium carbonate hexahydrate (ikaite) nucleated and stabilized in confined nano- and picovolumes. Cryst Growth Des 4:792–802. https://doi.org/10.1021/cg401672v
Rogov MA (2015) Glendonites in the Jurassic deposits of Northern Hemisphere. Jurassic system of Russia: problems of stratigraphy and paleogeography. In: Zakharov VA, Rogov MA, Ippolitov AP (eds) Fifth All-Russian meeting, September 15–20, 2015, Makhachkala, Scientific materials. pp 232–236. https://doi.org/10.13140/RG.2.1.1148.2083
Rogov MA, Ershova VB, Shchepetova EV, Zakharov VA, Pokrovsky BG, Khudoley AK (2017) Earliest cretaceous (late Berriasian)

glendonites from Northeast Siberia revise the timing of initiation of transient early Cretaceous cooling in the high latitudes. Cretac Res 71:102–112. https://doi.org/10.1016/j.cretres.2016.11.011

Rogov MA, Zverkov NG, Zakharov VA, Arkhangelsky MS (2019) Marine reptiles and climates of the Jurassic and cretaceous of Siberia. Stratigr Geol Correl 27(4):398–423. https://doi.org/10.1134/S0869593819040051

Rogov MA, Ershova VB, Vereshchagin O, Vasileva K, Mikhailova K, Krylov A (2021) Database of global glendonite and ikaite records throughout the Phanerozoic. Earth Syst Sci Data 13:343–356. https://doi.org/10.5194/essd-13-343-2021

Rogov MA, Ershova V, Gaina C, Vereshchagin O, Vasileva K, Mikhailova K, Krylov A (2023) Glendonites throughout the Phanerozoic. Earth Sci Rev 241:104430. https://doi.org/10.1016/j.earscirev.2023.104430

Ruebsam W, Al-Husseini M (2020) Calibrating the early Toarcian (early Jurassic) with stratigraphic black holes (SBH). Gondwana Res 82:317–336. https://doi.org/10.1016/j.gr.2020.01.011

Ruebsam W, Schwark L (2021) Impact of north-hemispherical cryosphere on early Toarcian climate and environmental perturbation. In: Reolid M, Mattioli E, Duarte LV, Ruebsam W (eds) Carbon cycle and ecosystem response to the Jenkyns event in the early Toarcian (Jurassic). GSL Special Publications 514. https://doi.org/10.1144/SP514-2021-11

Ruebsam W, Mayer B, Schwark L (2019) Cryosphere carbon dynamics control early Toarcian global warming and sea level evolution. Glob Planet Change 172:440–453. https://doi.org/10.1016/j.gloplacha.2018.11.003

Ruebsam W, Thibault N, Al-Husseini M (2020) Early Toarcian glacio-eustatic unconformities and chemostratigraphic black holes. In: Montenari M (ed) Stratigraphy and timescales—carbon isotope stratigraphy, vol 5. Elsevier, Amsterdam, pp 629–676. https://doi.org/10.1016/bs.sats.2020.08.006

Sadlok G, Zatoń M (2020) Ichnology of the Middle Jurassic hiatus concretions from Poland: implications for their formation, exhumation, and palaeoenvironment. Palaeobiodivers Palaeoenviron 100(3):757–771. https://doi.org/10.1007/s12549-019-00410-6

Scheller EL, Grotzinger J, Ingalls M (2022) Guttulatic calcite: a carbonate microtexture that reveals frigid formation conditions. Geology 50(1):48–53. https://doi.org/10.1130/G49312.1

Schöllhorn I, Adatte T, van de Schootbrugge B, Houben A, Charbonnier G, Janssen N, Föllmi KB (2020a) Climate and environmental response to the break-up of Pangea during the Early Jurassic (Hettangian-Pliensbachian); the Dorset coast (UK) revisited. Glob Planet Change 185:103096. https://doi.org/10.1016/j.gloplacha.2019.103096

Schöllhorn I, Adatte T, Charbonnier G, Mattioli E, Spangenberg JE, Föllmi KB (2020b) Pliensbachian environmental perturbations and their potential link with volcanic activity: Swiss and British geochemical records. Sediment Geol 406:105665. https://doi.org/10.1016/j.sedgeo.2020.105665

Schubert CJ, Nürnberg D, Scheele N, Pauer F, Kriews M (1997) ^{13}C isotope depletion in ikaite crystals: evidence for methane release from the Siberian shelves? Geo Mar Lett 17:169–174. https://doi.org/10.1007/s003670050023

Schweigert G (2019) Die Schwanenfußmuschel jetzt auch aus Buttenheim. Fossilien 2019(1):30–33

Selleck BW, Carr PF, Jones BG (2007) A review and synthesis of glendonites (pseudomorphs after ikaite) with new data: assessing applicability as recorders of ancient coldwater conditions. J Sediment Res 77:980–991. https://doi.org/10.2110/jsr.2007.087

Stein CL, Smith AJ (1985) Authigenic carbonate nodules in the Nankai Trough, Site 583. Initial Rep DSDP 87:659–668. https://doi.org/10.2973/DSDP.PROC.87.115.1986

Stockmann G, Tollefsen E, Skelton A, Brüchert V, Balic-Zunic T, Langhof J, Skogby H, Karlsson A (2018) Control of a calcite inhibitor (phosphate) and temperature on ikaite precipitation in Ikka Fjord, southwest Greenland. Appl Geochem 89:11–22. https://doi.org/10.1016/j.apgeochem.2017.11.005

Suan G, Mattioli E, Pittet B, Lécuyer C, Suchéras-Marx B, Duarte LV, Philippe M, Reggiani L, Martineau F (2010) Secular environmental precursors to Early Toarcian (Jurassic) extreme climate changes. Earth Planet Sci Lett 290(3–4):448–458. https://doi.org/10.1016/j.epsl.2009.12.047

Suan G, Nikitenko BL, Rogov MA, Baudin F, Spangenberg JE, Knyazev VG, Glinskikh LA, Goryacheva AA, Adatte T, Riding JB, Föllmi KB, Pittet B, Mattioli E, Lécuyer C (2011) Polar record of Early Jurassic massive carbon injection. Earth Planet Sci Lett 312(1–2):102–113. https://doi.org/10.1016/j.epsl.2011.09.050

Suess E, Balzer W, Hesse KF, Müller PJ, Ungerer CA, Wefer G (1982) Calcium carbonate hexahydrate from organic-rich sediments of the Antarctic shelf: precursors of glendonites. Science 216:1128–1131. https://doi.org/10.1126/science.216.4550.1128

Surlyk F (2003) The Jurassic of East Greenland: a sedimentary record of thermal subsidence, onset and culmination of rifting. Geol Surv Den Greenl Bull 1:659–722. https://doi.org/10.34194/geusb.v1.4674

Swainson IP, Hammond RP (2001) Ikaite, $CaCO_3{\cdot}6H_2O$: cold comfort for glendonites as paleothermometers. Am Min 86:1530–1533. https://doi.org/10.2138/am-2001-11-1223

Teichert BMA, Luppold FW (2013) Glendonites from an Early Jurassic methane seep—climate or methane indicators? Palaeogeogr Palaeoclimatol Palaeoecol 390:81–93. https://doi.org/10.1016/j.palaeo.2013.03.001

Tollefsen E, Balic-Zunic T, Mörth C-M, Brüchert V, Lee CC, Skelton A (2020) Ikaite nucleation at 35 °C challenges the use of glendonite as a paleotemperature indicator. Sci Rep 10:8141. https://doi.org/10.1038/s41598-020-64751-5

van de Schootbrugge B, Richoz S, Pross J, Luppold FW, Hunze S, Wonik T, Blau J, Meister C, van der Weijst CMH, Suan G, Fraguas A, Fiebig J, Herrle JO, Guex J, Little CTS, Wignall PB, Püttmann W, Oschmann W(2019) The Schandelah scientific drilling project: a 25-million year record of Early Jurassic palaeo-environmental change from northern Germany. Newsl Stratigr 52(3):249–296. https://doi.org/10.1127/nos/2018/0259

Vickers ML, Watkinson M, Price GD, Jerrett R (2018) An improved model for the ikaite-glendonite transformation: evidence from the Lower Cretaceous of Spitsbergen, Svalbard. Nor J Geol 98:1–15. https://doi.org/10.17850/njg98-1-01

Vickers ML, Vickers M, Rickaby REM, Wu H, Bernasconi SM, Ullmann CV, Bohrmann G, Spielhagen RF, Kassensi H, Schultz BP, Alwmark C, Thibault N, Korte C (2022) The ikaite to calcite transformation: implications for palaeoclimate studies. Geochim Cosmochim Acta 334:201–216. https://doi.org/10.1016/j.gca.2022.08.001

Voigt E (1968) Über Hiatus-Konkretionen (dargestellt an Beispielen aus dem Lias). Geol Rundsch 58:281–296

Whiticar MJ (1999) Carbon and hydrogen isotope systematics of bacterial formation and oxidation of methane. Chem Geol 161:291–314. https://doi.org/10.1016/S0009-2541%2899%2900092-3

Zabel M, Schulz HD (2001) Importance of submarine landslides for non-steady state conditions in pore water systems—lower Zaire (Congo) deep-sea fan. Mar Geol 176(1–4):87–99. https://doi.org/10.1016/S0025-3227(01)00164-5

Zakharov VA, Shurygin BN, Il'ina VI, Nikitenko BL (2006) Pliensbachian–Toarcian biotic turnover in north Siberia and the Arctic region. Stratigr Geol Correl 14(4):399–417. https://doi.org/10.1134/S0869593806040046

Zhou X, Lu Z, Rickaby REM, Domack E, Wellner JS, Kennedy HA (2015) Ikaite abundance controlled by porewater phosphorus level: potential links to dust and productivity. J Geol 123:269–281. https://doi.org/10.1086/681918

Zimmermann J, Franz M, Heunisch C, Luppold FW, Mönnig E, Wolfgramm M (2015) Sequence stratigraphic framework of the Lower and Middle Jurassic in the North German Basin: epicontinental sequences controlled by Boreal cycles. Palaeogeogr Palaeoclimatol Palaeoecol 440:395–416. https://doi.org/10.1016/j.palaeo.2015.08.045

Zverkov NG, Grigoriev DV, Danilov IG (2021) Early Jurassic palaeopolar marine reptiles of Siberia. Geol Mag 158(7):1305–1322. https://doi.org/10.1017/S0016756820001351